Review

Bernard Gil*, Guillaume Cassabois, Ramon Cusco, Giorgia Fugallo and Lluis Artus

Boron nitride for excitonics, nano photonics, and quantum technologies

https://doi.org/10.1515/nanoph-2020-0225
Received April 3, 2020; accepted June 8, 2020; published online June 29, 2020

Abstract: We review the recent progress regarding the physics and applications of boron nitride bulk crystals and its epitaxial layers in various fields. First, we highlight its importance from optoelectronics side, for simple devices operating in the deep ultraviolet, in view of sanitary applications. Emphasis will be directed towards the unusually strong efficiency of the exciton–phonon coupling in this indirect band gap semiconductor. Second, we shift towards nanophotonics, for the management of hyper-magnification and of medical imaging. Here, advantage is taken of the efficient coupling of the electromagnetic field with some of its phonons, those interacting with light at 12 and 6 μm in vacuum. Third, we present the different defects that are currently studied for their propensity to behave as single photon emitters, in the perspective to help them becoming challengers of the NV centres in diamond or of the double vacancy in silicon carbide in the field of modern and developing quantum technologies.

Keywords: 2D materials; boron nitride; deep ultra violet emission; quantem technologies; single photon sources; wide band gap semiconductor.

> The health of semiconductor science, for all its many results in "pure" physics, continues to depend on its potential for application. *Alan B. Fowler Physics Today* 1993; **46**: 59

***Corresponding author: Bernard Gil**, Laboratoire Charles Coulomb (L2C), UMR 5221-CNRS-Université de Montpellier, F-34095 Montpellier, France, E-mail: Bernard.gil@umontpellier.fr. https://orcid.org/0000-0002-1588-887X
Guillaume Cassabois: Laboratoire Charles Coulomb (L2C), UMR 5221-CNRS-Université de Montpellier, F-34095 Montpellier, France
Ramon Cusco and Lluis Artus: Institut Jaume Almera (ICTJA-CSIC), Consejo Superior de Investigaciones Científicas, Lluís Solé i Sabarís s.n., 08028 Barcelona, Spain
Giorgia Fugallo: CNRS, UMR 6607, Laboratorie de Thermique et Energie de Nantes (LTeN) Polytech'Nantes, Université de Nantes, Rue Christian Pauc, F-44306 Nantes Cedex 3, France

1 The early days

Unexpected and incredible potentialities of hexagonal boron nitride (hBN) currently constitute the driving forces for its worldwide booming of interest in most of the advanced research laboratories studying the solid state and its applications. Researchers are focused towards various fields of investigations, among which are the developments of devices for information technologies, the imagination of various, environmental friendly eclectic applications, the conception and the realization of photonic devices dedicated to help for the diagnosis of biological and medical troubles, to cite a few examples. Nothing was predisposing hBN to this future. In 1842, the British Chemist W.H. Balmain [1] obtained a fragile powder through the reaction between boric acid (H_3BO_3) and potassium cyanide (KCN). This artificial compound sits among the oldest of the semiconductors like for instance ZnO (zincite was discovered by Sir Bruce Archibald [2] at the dawn of the nineteenth century) or Greenockite (CdS) [3] first observed in 1840 at Bishopton, Scotland and named according to the name of the landowner, Lord Greenock. In contrast to the two above cited crystals, hBN is one of these materials called III–V compounds semiconductors, which together with silicon are the crystals that, after being purified, doped, assembled together to form heterostructures, led to the developments of electronics, optoelectronics, computer science, in a word led to the settling of today's information technologies.

Using an optical microscope, the super-white powders obtained by Balmain revealed to be shaped as small and very thin platelets. This crystalline state triggered the first industrial interest noticed for hBN. The lamellar structure of the material makes gliding of adjacent reticular planes quite easy to produce and these hBN powders are industrially used for dried lubrication, like MoS_2 and/or in complement to it. The high melting temperature (about 2950 °C) of hBN and its chemical inertness were used for hot pressing the hBN powder in order to fabricate *microwave-transparent* growth crucibles that are today broadly used in synthesis that require high temperature operation.

The powders were also widely used as an additive in cosmetic recipes, from the middle of the last century till its end, before they were replaced by cheaper industrial solutions. We are very far from semiconductor-type applications although radio telecommunications were already demonstrated using other materials.

The thermal conductivity of hBN is very high [4–6], and it has stimulated modelling using semi-classical [4, 6–8] and quantum approaches [9, 10]. It is now fully understood and hBN is widely used for thermal management issues [11] in miniaturized devices or for thermoelectric applications [12].

It had been realized in 1930 that B could act as an efficient particle detector [13]. Some of the detected particles were later named neutrons following their identification in 1932 by Chadwick, the 1935 Nobel laureate in physics for the discovery of this neutron [14]. hBN is a good host crystal for neutron detection, and the performances of such detectors can be even enhanced if using ^{10}B monoisotopically purified boron, which is abundant in reasonable proportions in nature (20 per cent of natural B) [15]. The reasons for this enhancement are correlated to the interactions of neutrons with ^{10}B atoms with a cross section of 3835 barns to be compared with 0.0055 barns for ^{11}B. There are two boron neutron capture fission reactions possible with different probabilities of occurrence:

$$^{10}_{5}\mathrm{B} + n \rightarrow {}^{7}_{3}\mathrm{Li}\,(0.83\,\mathrm{MeV}) + \alpha\,(1.47\,\mathrm{MeV}) + \gamma\,(0.48\,\mathrm{MeV}) + 2.31\,\mathrm{MeV}\,(94\%)$$

$$^{10}_{5}\mathrm{B} + n \rightarrow {}^{7}_{3}\mathrm{Li}\,(1.01\,\mathrm{MeV}) + \alpha\,(1.77\,\mathrm{MeV}) + 2.79\,\mathrm{MeV}\,(6\%)$$

2 The new era of hBN

Decisive scientific breakthroughs appeared when large size (about $1 \times 1 \times 0.2$ mm^3) single crystals were grown in 2004 in the group of T. Taniguchi at NIMS [16] and later in the groups of James Edgar at KSU [17], Nikholai Zighadlo at Basel University [18] and many other actors including several companies now selling it. Watanabe et al. [16] demonstrated in particular in their 2004 article that hBN could emit a strong cathodoluminescence signal at 215 nm and that laser action could be observed at this short wavelength, a wavelength never reached before. In addition, they realized a bulky demonstrator that was published in 2009 [19]. The interest for hBN has been really boosted in various areas and today millimetre size single crystal platelets are routinely obtained by growers and are available in the catalogues of crystal suppliers.

Since that, actors operating in different area of the science of devices for information technology have been rapidly coming into the play, and at the time being, hBN is world-widely used for different kinds of research. The bulk crystals have been of value for measuring the refractive indices [20], the stiffness coefficients [21], refining the Infra-Red signature of phonon energies [22] in polarization conditions [23] and they have triggered a lot of photonic applications in the near infrared [24]. These applications include:

- hyper-lensing effects useful in nanomedecine [25]. They are based on the specificities of hyperbolic dispersion relations near the phonon frequencies [26, 27],
- taking advantage of the zero-value of the group velocities at some specific wavelengths of Reststrahlen bands [28].

The lamellar structure of the material makes gliding of adjacent reticular planes easy, enabling the use of hBN (and also graphite) as a release layer between an active nitride-based device and the expensive high-quality substrate used to grow it [29]. The idea is to split both partners after the device has been fully processed for further reusings of the substrate. This easy cleavage property is now extensively used by people working in the area of 2D materials and hBN is world-widely utilized as a passivation layer for different few-monolayer stacking of transition metal dichalcogenides, GaSe, InSe, black phosphorus, and so on [30, 31].

Also of interest is the ultra-short emission wavelength at 215 nm which clearly sits at a wavelength substantially shorter than what can be achieved using the ultimate challenger heterostructure based on a gallium plane embedded into AlN barrier layers (235 nm at 8 K) [32]. Although a lot of efforts are at the time being focused towards the 260–270 nm range [33, 34] where light absorption by DNA molecules is important, hBN-related devices will be of paramount importance for fully covering the 200–300 nm range for nucleic acids (DNA and RNA) where the UV absorbance is due to transitions of the planar purine and pyrimidine bases (see Figure 1 where the wavelengths that can be attributed to GaN-AlN devices are yellowed while the region of hBN-related ones is greyed) [35]. The detailed analysis of light–matter interaction for DNA in the 200 nm range when the system is photo-perturbed (like for instance under a dense photoexitation) is living its infancy. A bright future is thus expected for hBN light emitters used as efficient DNA breakers that are good to directly kill viruses-like COVID-19 for instance and it is also efficient to jeopardize the existence of bacteria propagating nosocomial diseases.

For all these reasons and also beyond them, the yearly number of citations that can be counted using the BN acronym is currently exponentially booming [36].

Creating and developing a technology requires growing large areas of high quality materials using epitaxial techniques like Metal Organic Chemical Vapour Deposition (MOCVD) or Molecular Beam Epitaxy (MBE). There are currently a lot of worldwide attempts among which are the pioneering works in the groups of H.X. Jiang at Austin (MOCVD) [37], S.V.Novikov at Nottingham (MBE) [38] and D. Jena at Cornell [39]. Epitaxial hBN can be grown with different thicknesses from the monolayer (MLBN) to very thick stacking. We have shown that the band gap of MLBN is direct at K in reciprocal space [40] while the fundamental band gap of bulk hBN is indirect between M and K points of the first Brillouin zone [41, 42]. The high internal quantum efficiency is correlated to the strong exciton–phonon coupling with an efficient and fast phonon emission that relaxes the k-dependent selection rule traditionally preventing indirect band gap semiconductors to strongly emit light *via* intrinsic processes [43–48]. This intriguing specificity of hBN is currently under active study, including the physics of the free and bound excitons.

In their seminal work, Arnaud et al. [43] have proposed a first calculation of the Coulomb interaction between electrons and holes, which they found very large and interpreted in favour of a Frenkel-type indirect exciton. This led to several theoretical calculations for hBN monolayers and bulk crystals. They have been of increasing complexities with time passing [49–53]. Intentional substitutional doping of hBN with foreign atoms is very much challenging [54], incorporation of C, Si, and Mg have been attempted with moderate fortunes

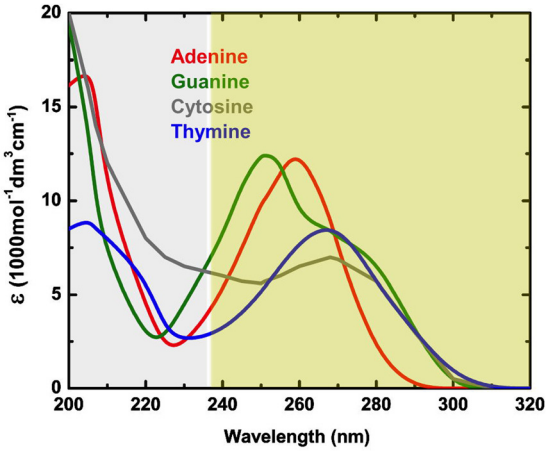

Figure 1: UV spectra of the DNA nucleotides (This figure is partly plotted from data published reference [35]).

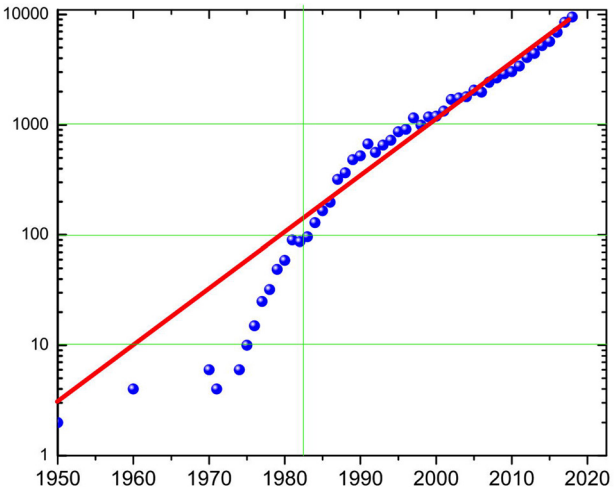

Figure 2: Yearly number of citations obtained using the Web of Science and the acronym « BN »

[55]. The bulk material is still particularly rich in different defects, which is fortunate as many of them act as efficient single photon sources [56–60]. They browse a broad energy range from let us say 5.5 eV down to about 1.5 eV and they are on the go towards an identification in terms of "what gives what" [61, 62].

These introduction sections come to their end. Before to skip to the next sections for more detailed discussions, we would like to encourage readers to join the hBN related activity: using as an indicator "BN" in the "topics" window of the Web of Science, the software reports a yearly exponential increase of the number of citations reported in Figure 2, attesting for the health of hBN-related research.

3 The crystalline state of hBN

The centro-symmetric D_{6h} ($P6_3mmc$ space group) symmetry of hBN was established in 1950 by R.S. Pease who disentangled many controversial proposals [63]. The lattice of hBN consists of a stacking of reticular planes of B_3N_3 hexagons made of alternating **tightly bound** B and N atoms with interatomic spacing of 0.1446 nm. B and N atoms in planes of ranks x and x + 2 stacked along the high order symmetry axis are exactly superimposed at 0.666 nm while atoms N and B of plane of rank x + 1 are exactly sandwiched between atoms B and N respectively of the planes of rank x and x + 2. The bonds along the c direction are loose and their weakness is the evidence of van der Waals bonding. This stacking is named AA′ where the prime label indicates a rotation of 60° of the hexagons

between the different adjacent planes to distinguish the orientation of planes of rank x from the orientation of plane of rank x + 1. This identification was made possible to R.S. Pease after careful analysis of the relative intensities of the different peaks of the diffraction patterns of hBN that he published two years after his initial report [64]. He also demonstrated experimentally a contraction (respectively a dilatation) of the in-plane (respectively on-axis) lattice parameter when increasing T. Using a modern X-ray diffractometer, after a large and accurate sampling of the reciprocal space of hBN, Arie Van der Lee managed to obtain the density of electrons that was published in [23] and which is offered in Figure 3. The determination of this AA′ stacking was far from trivial as there exists a lot of very close hexagonal polytypes (see Figure 3) that correspond to very similar values of the in-plane lattice parameter a and slightly different values of c [65–67]. These polytypes will have different band structures for electrons [65] and phonons and different excitonic energies [53]. We will restrict here our article to the AA′ stacking or to monolayers, the cubic wurtzitic and rhomboedral phases will not be discussed either. In graphite, there is an in-plane translation between alternating planes of the stacking so that half the atoms lie between the centres of the hexagonal rings of adjacent layers, which is very similar mutatis mutandis to the AB_1 stacking of boron nitride. *Starting from now, we will here strictly restrict the hBN acronym to the AA′ stacking.*

In Figure 4(a) is plotted a side view of the atomic arrangement for a monolayer of BN, for which the symmetry is D_{3h}. The plane of the monolayer contains all atoms and it is a symmetry plane. As the main symmetry axis perpendicular to the symmetry plane is threefold, there is no inversion symmetry; therefore, group theory allows piezoelectricity [68, 69]. In Figure 4(b) is plotted a bilayer of hBN for which the symmetry is D_{3d}, leading to a non-piezoelectric crystal as this drawing is centrosymmetric (the centre for inversion symmetry is at the middle of the two planes). As can be seen in Figure 4(c) a three-layer ML sample looses inversion symmetry, although the central layer contains a symmetry plane. Few layer hBN stacking are alternatingly piezoelectric (odd number of monolayers) or not (even numbers of monolayers). This leads to a rich physics for the light matter interaction processes.

In the left hand side of Figure 5 is plotted the three dimensional atomic arrangement of hBN. Boron atoms are plotted as yellow spheres and nitrogen atoms as blue ones. The vectors of the lattice unit cell are represented using dashed red lines and the vectors of the reciprocal lattice are plotted as dashed purple lines. The vectors of the International basis (**x**,**y**) and ($\mathbf{k_x}$, $\mathbf{k_y}$) are also indicated. In the right hand side is plotted the Brillouin zone (green) with notations of specific points is plotted the plane view of a BN monolayer.

Three important results have to be underlined here:

- Along the $\mathbf{k_x}$ direction, lines made of nitrogen and boron atoms alternate. This will open the band gap of monolayer BN at **K** whilst the band gap of graphene (and graphite) will be closed at K as there will be no alternance with a single carbon atom.
- Along the $\mathbf{k_y}$ direction there are lines made of alternating nitrogen and boron atoms with alternating long and short interatomic spacings. In graphene (and graphite), this alternance of long and short carbon interatomic spacing exists. Therefore, the band gap at **M** is open for both materials.
- There are couples of geometrically equivalent points **K** and **K′** (**M** and **M′**) in the Brillouin Zone. The impact of this geometrical degeneracy that is lift for **K** and **K′**

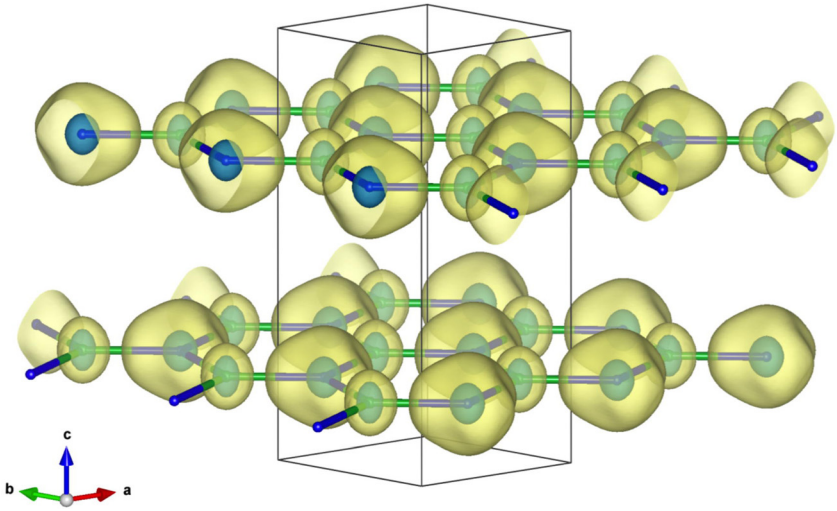

Figure 3: The side view (view orthogonal to c-axis) of the electron density reveals the AA′ stacking of h-BN. This projection is obtained from the X-ray diffraction pattern using the maximum entropy method. Reproduction of figure S7 of reference [23].

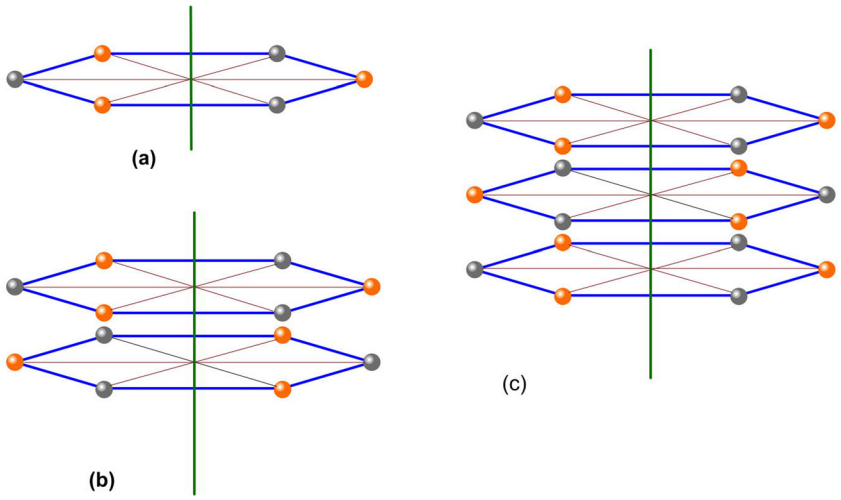

Figure 4: BN monolayer (a), bi-layer AA′ stacking (b) and three layer AA′ stacking. Boron atoms are plot as orange spheres and nitrogen atoms are greyed ones. The c axis is vertical.

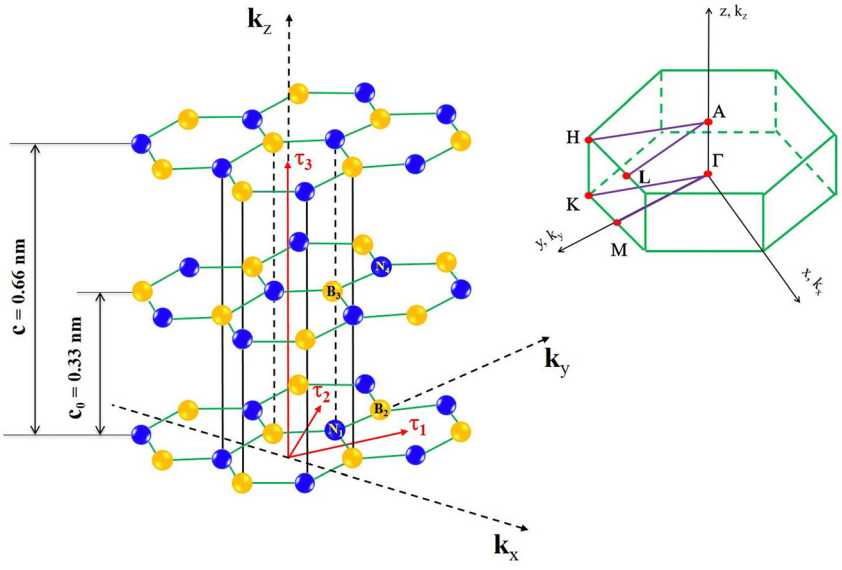

Figure 5: (Left): Plot of the three dimensional atomic arrangement of hBN. Boron atoms are plotted as yellow spheres and nitrogen atoms as blue ones. The vectors of the lattice unit cell are represented using dashed red lines and the vectors of the reciprocal lattice are plotted as dashed purple lines. The vectors of the International basis (x,y) and (kx, ky) are also indicated. (Right) Plot of the Brillouin zone (green) with notations of specific points. Courtesy Dr. Thi Quynh Phuong Vuong.

under time reversal symmetry is at the origin of the valley physics, and explains chiral selection rules. It has been reviewed in [70] for ultra thin Transition Metal Dichalcogenides.

4 Lattice vibrations of hBN

4.1 BN powders paved the way of nanophotonics with hyperbolic polaritons

If we consider the point symmetries encountered for the monolayer, the bilayer, or bulk hBN, their multiplication tables always discriminate symmetries in the plane from symmetries along the c direction [71, 72]. A detailed group theory analysis, very useful for electronic and phononic band structure calculations, has been published by Goñi and Pastori Parravicini [73]. The symmetries of the eigenmodes of in plane and on axis lattice vibrations at zone centre (as well as their selection rules for infrared excitation or Raman inelastic light scattering) and at zone edge are different and they were predicted and identified by Geick et al. [74] and will be re-addressed in details in the next section. Their identification still holds and was inferred by other works which essential ones are [75–79] and which were all performed using powders or very tiny crystals. An important result to outline is the determination of the real and imaginary parts after Kramers–Krönig analysis of the reflectance near the infrared transitions corresponding to the two E_{1u} modes at 783 and 1367 cm^{-1} under **E**//**c** and **E**⊥**c** polarizations [74]. We have reproduced in Figure 6a,b, using blue lines, the spectral

dependences of the real part of the dielectric constant for these Infrared active modes obtained using the data of this reference. The atomic displacements are added in Figure 6c. It appears that the real parts of the dielectric constant can take large negative values in the range of wave numbers in a first Reststrahlen band between 784 and 819 cm^{-1} (about 12 μm wavelength) for **E//c** while is simultaneously positive in the other polarization. Similarly it appears that the real part of the dielectric constant can take **huge** negative values in the **broad range** of wave numbers in a second Reststrahlen band between 1367 and 1607 cm^{-1} (about 6 μm wavelengths) for **E⊥c** while it is simultaneously positive in the other polarization. In these experiments on powders Geick et al. [74] have evidenced, without noticing it, the importance of hBN for Infrared nanophotonic applications based on hyperbolic phonon polaritons that were going to be proposed some years later [24–28, 80–83].

In the simplest case of a uniaxial crystal with an anisotropic dielectric constant like in the case of hBN, the dispersion relation for the phonon polaritons (the mixed state resulting of the phonon with the electromagnetic field, both having the same energy) writes in terms of a nontrivial form [80]:

$$\frac{\omega^2}{c^2} = \frac{k_z^2}{\varepsilon_{xx}} + \frac{k_x^2 + k_y^2}{\varepsilon_{zz}}$$

Depending on the relative values and on the sign of the components of the dielectric constant the dispersion relation probes a surface with characteristics of a sphere, an ellipsoid or two kinds of hyperboloid surfaces as indicated in Figure 7. In the first Reststrahlen band, the on-axis and in-plane values of the dielectric constants switch their signs: $\epsilon_{zz} < 0$ and $\epsilon_{xx} > 0$ while in the second one, $\epsilon_{xx} < 0$ and $\epsilon_{zz} > 0$. As a consequence there are very different hyperbolic polaritons in these two Reststrahlen bands.

Advantage can be taken of:

- The huge value of the dielectric constant to squeeze the wavelength of the infrared light for instance in the ~12–~6 μm range
- The hyperbolic dispersion relation in the space of wavenumber to generate specific photonic effects [24–28, 80–83]

Using bulk crystals, and re-handling, the measurement on large single crystals we have recently measured the polarized spectral dependences of the dielectric constant that can be modelled using Lorentzian functions having significantly different values of the oscillator strengths and broadening parameters [22], giving in particular more huge negative values of the dielectric constant for wavelengths in the ~6 μm range, as can be seen in Figure 6a, b. To the best of our knowledge, these huge negative values of epsilon that can only be generated in other semiconducting materials after expensive and tricky processing are not naturally observed for other bulk semiconductors of technological interest, in these wavelengths. This new set of values indicates that quantum nanophotonics based on BN at 6 μm is squeezing the infrared length to dimensions much smaller than thought from the using of parameters of reference [74].

4.2 Bulk single crystals

With the advent of bulk single crystals sometimes monoisotopically purified, it has been necessary to examine in

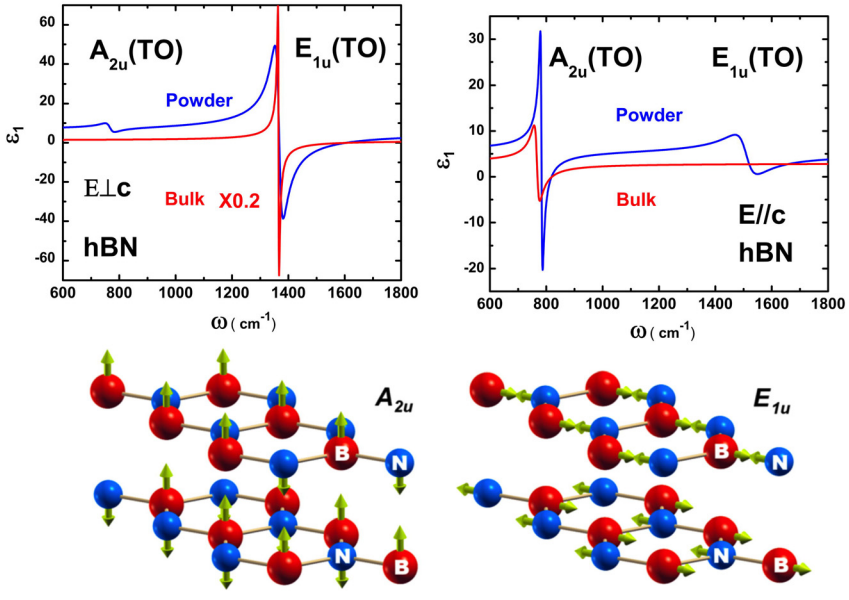

Figure 6: (a) Real part of the dielectric constant for the low frequency intfrared active mode at 783 cm^{-1} (blue) and (b) for the high frequency mode at 1367 cm^{-1} (red). Note the negative values in the Reststrahlen band. (c) Atomic motions of the out-of-plane (A_{2u}) and in-plane (E_{1u}) IR-active modes of h-BN. This figure is plotted from numerical data taken in references [22, 74].

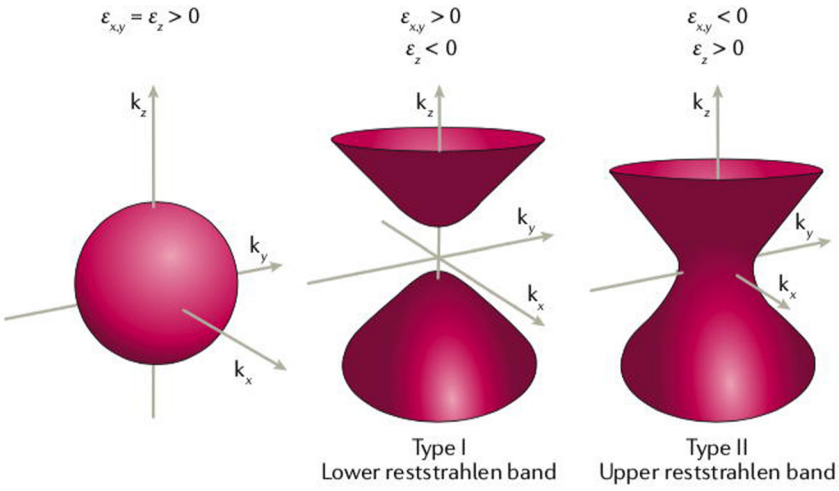

Figure 7: Isofrequency surface $\omega(k_x,k_y,k_z)$ =cte in the 3D-space, for an isotropic medium($\varepsilon_{xx} = \varepsilon_{yy} = \varepsilon_{zz>0}$) and a hyperbolic medium with dielectric or type I ($\varepsilon_{xx \text{ and }} \varepsilon_{yy} > 0$, $\varepsilon_{zz} < 0$) and metallic or type II ($\varepsilon_{xx \text{ and }} \varepsilon_{yy} < 0$, $\varepsilon_{zz} > 0$) response. This is a reproduction of figure in box 2 after reference [25].

details what are the numbers that can account for the physics of the phonons in hBN crystals of improved structural quality, that is to say with qualities high enough to reach observations of pure selection rules and with reduced inhomogeneous broadening effects. We also investigated the temperature dependences of the lattice vibrations. This impacts the understanding of confined hyperbolic polaritons already discussed in the preceding: a good knowledge of phonons in hBN is essential for using long-lived phonon–polariton modes in the perspective of nanophotonic applications in the 6 μm range. Developing solid-state neutron detectors with improved device architectures and higher detection efficiencies can also benefit of such knowledge in the specific case of ^{10}BN. We have focused on the specific case of phonon energies and broadenings under temperature and versus isotopic composition. There are many theoretical calculations of the normal vibration modes and elastic constants in hBN, which were produced with models of increasing complexities, as extensively discussed in references [84–95].

To the *P*6$_3$/*mmc* space group of hBN bulk crystals corresponds the D_{6h} point group. This point group is centrosymmetric and, consequently, the modes that are Raman active are not IR active and vice versa. The unit cell of bulk hBN contains four atoms, and therefore 12 different modes exist. From these, nine are optical modes which decompose at the Brillouin zone centre as $E_{1u} + A_{2u} + 2\ E_{2g} + 2\ B_{1g}$. According to group theory, E_{1u} and E_{2g} representations are doubly degenerate, whereas the A_{2u} representation is non-degenerate. The basis functions of the irreducible representations indicate that the B_{1g} modes are silent, the E_{1u} and the A_{2u} ones are IR active and the E_{2g} modes are Raman active. In Figure 8, the eigenvectors of all these optical modes are displayed. For both E_{2g} modes, the motion of all B and N atoms takes place in the hexagonal layers perpendicular to the c axis. However, their frequencies substantially differ. In one case, the B atoms vibrate against the N atoms in the in-plane honeycomb structure, giving rise to high-frequency modes denoted as $E_{2g}{}^{h}$ modes. In the other case, the B and N atoms move in phase within a given layer but the atomic displacements in adjacent layers have opposite phase, resulting in an interlayer gliding motion. Consequently, this mode presents a very low frequency and is denoted as $E_{2g}{}^{l}$. The centre of the electrical charge is invariant in both cases, and, consequently, both are non-polar modes that do not present IR activity. In contrast, the E_{1u} modes and the A_{2u} modes are polar since they present a net displacement of the electrical charge, and, consequently, they exhibit IR activity. While in the E_{1u} modes the atomic motion is restricted to the hexagonal layers (in-plane vibration), in the A_{2u} modes, B and N atoms vibrate against each other along the c-axis direction (out-of-plane vibration) (see Figure 8). As a consequence, and taking into account that z is a basis function of the A_{2u} irreducible representation whereas x, y are basis functions of the E_{1u} irreducible representation, the A_{2u} modes are allowed for incident light polarized parallel to the c axis whereas the E_{1u} modes are allowed for incident light polarized perpendicular to the c axis. The temperature dependence of phonons yields relevant information about the electron-phonon interaction, which determines the energy-loss rate from electrons to the lattice *via* phonon emission and is a key parameter in the design of high-speed devices. At high current densities, the energy loss of hot electrons to the lattice gives rise to self-heating effects that are deleterious to device performance. Depending on the phonon lifetimes, a non-equilibrium hot-phonon population may build-up, leading to phonon reabsorption and a reduction of the carrier energy-loss rate. Therefore, a good understanding of the

optical-phonon decay processes into acoustic phonons is a key element to address self-heating effects in optoelectronic devices and to devise phonon-engineering strategies to lessen its impact on device performance. Additionally, the decay of zone-centre phonons can generate a high population of large-wave-vector phonons that may facilitate momentum conservation in nonradiative Auger processes thus causing severe limitations to the internal quantum efficiency of light emitting devices. Although experimental Raman and IR measurements only allow the determination of the respective active-mode frequencies at the Brillouin zone centre because of the wave-vector conservation selection rule, it is important to have a good knowledge of the dispersion of all the phonons throughout the entire Brillouin zone.

There are two pairs of twice-degenerated Raman active modes of E_{2g} symmetry in hBN, which are measured typically at 52.7 and 1369 cm^{-1} in ^{nat}BN at 77 K [92]. The atomic displacements corresponding to these vibrations are reproduced in Figure 8. When increasing T the low energy mode softens due to the increase of the interlayer spacing and the narrow experimental signature of this Raman line does not broaden for temperatures up to 600 K [92], due to the lack of phonon dissociation channels. In line with the measurements of Pease [64], as the in-plane lattice parameter decreases with increasing T, one may expect an increasing frequency of the high energy mode with T that is not observed experimentally. This unconventional behaviour is predicted by DFT calculations [92]. At this stage, it is mandatory to have a closer look to the physics underlying the observed phenomenon. In complement to this temperature dependence, it is convenient to examine the behaviour of the full width at half maximum of this high-energy mode. We measured a significant enhancement with increasing T. From the qualitative side, the finite lifetime of the phonons as they decay into phonons in other branches through anharmonic processes that conserve energy and crystal momentum give rise to a temperature-dependent broadening of the Raman line. To explain this quantitatively in hBN, it requires taking into account quartic anharmonicity in the phonon decay processes [93], which is not a trivial task and which is also of paramount importance for explaining the temperature-induced softening of this Raman mode. This softening is characteristics of the layered nature of hBN and graphite and it is correlated to the existence of very low frequency modes associated with weak interlayer interactions, and to the specific coupling between the low frequency and high-frequency Raman modes of hBN. We refer to [92] for in-depth discussion of this very technical issue.

This peculiar layered structure leads also to a highly anisotropic thermal conductivity. If it is true that measurements of thermal conductivity in hBN are available since the 70s [5, 6, 10], it is also true that quite some discrepancies can be found in experimental estimations. The primary challenge in measuring the thermal conductivity of h-BN single crystals is that the typical size of the single crystals is not large enough for many characterization techniques [94]. Moreover due to porosity present in the first samples measured [5, 6] it is even unclear if the discrepancies observed are due to inconsistencies in measurement methods or rather in sample quality. On the theoretical side, ab *initio* calculations based on Boltzmann transport theory (BTE) [95–97] have demonstrated high accuracy in describing thermal conductivity of a variety of bulk materials, but for the specific case of hBN while monolayer got immediately a lot of attention for its high thermal conductivity [9, 98] it is only in 2018 that we can find a first exhaustive *ab initio* BTE study of bulk hBN [10]. In this joint experimental and theoretical study the authors

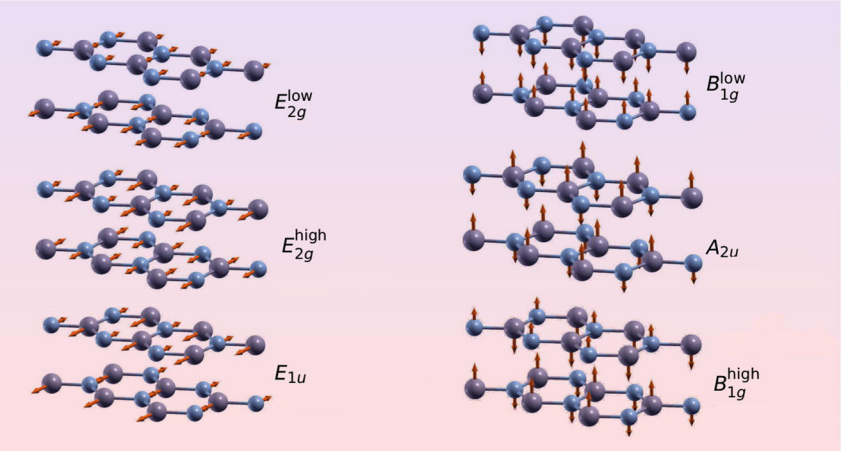

Figure 8: Sketch of the atomic displacement of the nine optical phonons of hBN. E_{1u} and E_{2g} modes are twice-degenerated.

find, as expected, a $1/T$ dependence for the in-plane-thermal conductivity (k_p) for T > 300 K while for the out-of-plane case (k_z) this usual trend is not observed. On the contrary, a rather flat dependency is found both experimentally and numerically. Moreover, on the opposite of what normally observed and found also for the in-plane case, k_z shows a larger reduction due to phonon-isotope scattering at higher temperatures (T > 300 K) than at lower ones. These unusual behaviours of k_z can be explained in terms of the different contributions of the low frequency modes (showing a 1/T dependence) and high-frequency ones (increasing with increasing temperature). While the entire temperature range of k_p is dominated by contributions from low frequency modes, these modes make comparable or even lower contributions to k_z than high frequency ones at higher temperatures. As these high-frequency modes become more important in k_z at high temperatures, so does the phonon-isotope scattering that these modes are more susceptible to [10] justifying the different trends observed between the in-plane and out-of-plane thermal conductivity.

Changing ^{11}B by ^{10}B produces a 10% change in the cation mass. We therefore expect huge modifications of the phonon energies compared with what can be found in GaN [99]. In Figure 9(a) is plotted the high energy Raman mode measured at 300 K for hBN grown using natural boron, ^{10}B and ^{11}B. One observes a softening of this Raman modes from ^{10}BN to ^{11}BN as expected from the classical equation between the pulsation of the harmonic oscillator ω, the force constant k and the reduced mass μ: $\omega = \sqrt{\frac{k}{\mu}}$. Here, changing the isotope from ^{11}B to ^{10}B decreases the reduced mass for the vibrating B and N pair and enhances almost linearly ω when increasing $\sqrt{\mu}$. However, for the sake of the completeness there is a slight departure from linearity to promote a sublinear behaviour in the ^{10}B-rich region, as an evidence of the modification of k in the naive equation above, due to anharmonic effects. We also remark a reduction of the full width at half maximum when the isotopic disorder in the boron lattice is suppressed in mono-isotopically purified samples.

To understand these effects, we performed high resolution X-ray diffraction and Raman scattering experiments as a function of T of ^{10}BN and ^{11}BN and we find different behaviours which permit, when combined with our calculations, to understand why ^{10}BN is more appropriate than ^{11}BN for designing devices using confined hyperbolic polaritons. A specific paper namely reference [100] is dedicated to the investigation of these isotopic effects on Raman modes of hBN versus temperature.

Three quantities need to be understood:

- The evolution of the energies of the phonon modes with isotopic proportions
- The value of full width at half maximum in correlation with isotopic proportions and against the disorder in the boron sublattice
- The evolution of anharmonic effects with isotopic proportions

Works on ^{nat}BN are gathered with data taken on ^{10}BN and ^{11}BN. In Figure 10 are reported the dispersion relations computed for ^{10}BN (blue lines) and ^{11}BN (red lines) samples. Eigen vectors corresponding to Raman-active (E_{2g}) and Infrared active (A_{2u} et E_{1u}) are also plotted. The dispersion relations are derived from group theory considerations and they are *mutatis mutandis* similar to what we computed for ^{nat}BN [92] or to what are found for the graphene/graphite-related case [86, 91]. In Figure 10, the phonon dispersion and the phonon density of states in hBN obtained from density functional theory (DFT) calculations are shown. Along the in-plane Σ and T lines, the E_{2g} modes split into LO and TO branches (labelled LO_1 and TO_1 for the low-energy mode and LO_2 and TO_2 for the high-energy mode). Similarly, the polar E_{1u} mode gives rise to the TO_3 and LO_3 branches, with a sizeable LO-TO splitting at zone centre. The c-axis polarized B_{1g} mode gives rise to the optical branches labelled as ZO_1 and ZO_3, corresponding to the low-energy and high-energy modes respectively, and the A_{2u} mode gives rise to the ZO_2 branch. In Figure 10, the different phonon branches are labelled using this systematic scheme [48, 74, 92], which will allow us to unambiguously identify the phonons that participate in the phonon-assisted emissions. There are three pairs of

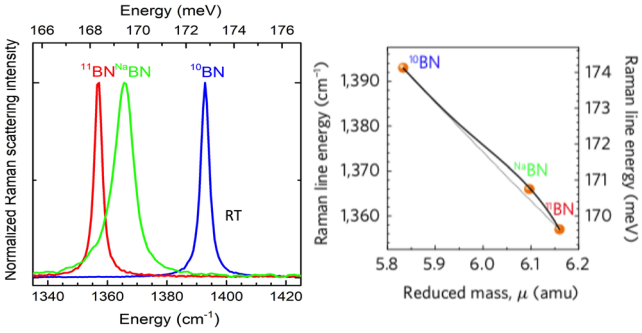

Figure 9: (a) Raman features obtained at room temperature for BN grown with natural boron ^{Nat}B (green), ^{11}B(red) and ^{10}B(blue) monoisotopically purified boron. (b) Plot of the energies measured for the high frequency Raman active phonon versus the reverse of the reduced mass μ ($1/\mu = 1/m_N + 1/m_B$ where m_N and m_B are the nitrogen and atomic masses repectively). After Figure 1b,c of reference [119].

branches, namely TA and TO_1, LA and LO_1, and TO_2 and TO_3 that derive from different zone centre modes and they are non-degenerate at finite **q** although the branches are very close in frequency within each pair. These quasi-degenerate parallel phonon branches can be better understood by observing carefully the region close to the Γ point. At zero frequency, we can find the two degenerate TA and LA modes with E_{2u} symmetry, while 6 meV above their Davydov partner TO_1 and LO_1 with E_{2g} symmetry. At finite q, the degeneration disappears and the two couples of branches split in two non-degenerates ones of symmetry A_1 (LA TO_1) and B_1 (TA LO_1). The two A_1 modes mix via an avoided crossing and then approach their respective B_1 mode forming in this way two Davydov pairs with a tiny energy splitting. It is interesting to notice that while at zero the 6 meV splitting is due to constructive interference of the Fourier components of the inter-layer interaction, the low splitting values at finite q are associated to the destructive interference of the Fourier components of this inter-layer interaction.

DFT calculations reveal that ^{10}B isotopic substitution in hBN yields an upward shift of the ^{11}BN phonon bands, which is most marked in the high energy optical modes (≈35 cm^{-1} for higher energy modes of E_{2g} and E_{1u} symmetry), whereas the acoustic modes show very little sensitivity to isotopic substitution throughout the Brillouin zone.

In hBN crystals with a random distribution of boron isotopes, the mass fluctuations in the boron sublattice break the translational symmetry, and momentum conservation laws are relaxed. This allows elastic scattering of phonons, leading to a phonon self-energy renormalization and to the formation of a low energy tail of the density of states resulting in an asymmetry of the Raman line in favour of its low energy tail. This is very similar to what is found for electrons in alloys [101], explaining why phonon lines are broader in ^{nat}BN than in isotopic BN. This also quantitatively explains the departure of the phonon energies from the values that are predicted by the virtual crystal approximation. Phonon lifetimes are related to the Raman line width via the energy–time Heisenberg uncertainty principle. A substantial increase in phonon lifetime by nearly a factor of three is observed in isotopically pure samples as deduced from Figure 9(a).

The impact of isotopic substitution on the anharmonic decay channels has also been investigated. The uneven shift of the phonon bands has implications on the phonon anharmonic decay channels, which for ^{10}BN include a relevant decay path into two phonons [102] that has a more prominent role than in ^{11}BN and ^{nat}BN for which the quadratic anharmonicity process dominates. Arguments pleading for these different processes are brought by the theoretical calculations and experimental facts. Number one, in ^{10}BN, the whole series higher energy phonon spectra match better (for the decay into two phonons while it is not the case for ^{11}BN and ^{nat}BN). This is in relationship with energy considerations and the global ≈35 cm^{-1} shift of the high energy phonons. Number two, one observes a clear the symmetric Raman line shape in the experiments on the ^{10}BN crystal while it is not the case for ^{11}BN and ^{nat}BN. The phonon lifetime values that are obtained at room temperature are only slightly higher than those reported in Ref. [82]. The estimations of the intrinsic phonon lifetime for isotopically pure hBN are roughly a factor of two lower than the *ab initio* theoretical predictions given in Ref. [82]. Thus, the expectations of achieving substantial polariton propagation lengths by reducing back-ground impurity concentration in hBN, where group velocity at which the polariton propagates can be exceptionally slow, appear to be more limited than suggested in this paper. With increasing temperature, the phonon lifetime decreases and the differences between the intrinsic phonon lifetime and the full phonon lifetime as well as the differences between

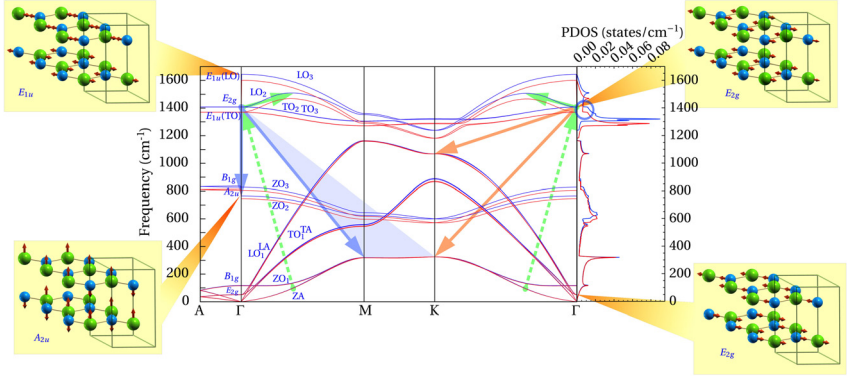

Figure 10: Phonon dispersion along the main symmetry lines and the corresponding phonon density of states for isotopically pure ^{10}BN (blue lines) and ^{11}BN (red lines). Encircled is the step-like ridge in the phonon density of states around the frequency of the high-energy E_{2g} mode. The main phonon decay channels (see text and reference [100]) are indicated by arrows. The atomic motions of the E_{2g} Raman-active modes as well as those of the infrared active modes (E_{1u} and A_{2u}) are illustrated. The atomic displacement corresponding to IR-active modes and Raman active modes are placed in the left-hand and right-hand sides of the central figure respectively. This figure is a reproduction of Figure 2 in reference [100].

isotopically pure and natural composition samples are reduced. Switching our attention back to Figure 6, the breakdown of the optical selection rules for Infrared Active transitions (A_{2u} and E_{1u} phonons) in reference [74] reveals the polycrystalline character of the studied samples, which implies that contributions from both modes are present in each polarized reflectivity spectra regardless of the electric field polarization. An unrealistically high damping value was also reported, which is incompatible with the large phonon-polariton propagation lengths recently measured in hBN [82]. Moreover, the $\varepsilon(0)$ and $\varepsilon(\infty)$ values reported by Geick et al. [74] are quite similar for both $E \perp c$ and E//c polarizations due to the contribution of both modes in each polarization. The similarity in the reported values is not consistent with the huge anisotropy observed in layered hBN [22], which reveals substantial differences between the in-plane and out-of-plane dielectric responses. We believe that many modelling of devices based in hyperbolic polaritons should now be re-handled, as there is substantial room for improving by design the quality factor of the optical response of devices by using the bulk values of the dielectric constant of hBN.

Isotopic purification can increase the room-temperature thermal conductivity of hBN with isotopic enrichment in excess of 100% [103], which could boost the values of K_r of reference [6, 10] to the record value of about 850 $Wm^{-1}K^{-1}$ at 300 K and K_z would reach 10 $Wm^{-1}K^{-1}$, still at 300 K. Obviously hBN could be fruitfully used as a substrate where thermal management issues are important like for perovskite lasers. However, this requires to be consolidated from the theoretical side before growers could think of it.

In the area of the spectroscopy of monolayer transition metal dichalchogenides, some recent papers [104, 105] indicate the co-existence of several kinds of phonon-assisted transitions which involve phonon at specific points of the Brillouin zone, which is in the spirit and in the continuation of what we found earlier in bulk hBN [106].

5 Excitons in hBN

5.1 Deep ultraviolet photoluminescence and efficient exciton-phonon interaction processes in bulk BN

From the early days, the fluorescence, photoluminescence (PL), cathodoluminescence (CL) spectra of hBN have been peaking at 5.5 eV (red part of the plot in Figure 11). This has long been luring the physicists, and it has long been misleading their interpretations. Little attention was paid to the weak and high energy levels plotted in blue in the figure, although Watanabe et al. [107] focused part of their attention to them and tried to make an identification of their origin. These lines are sitting at energies well below the singularities of the dielectric constant that Hoffman et al. [79] had detected at 6.1 eV and above. In addition, the band at 5.3 eV reveals a dual contribution (see inset in Figure 11), as another evidence of hidden complexities. The severe difficulties that had long been hurdling a perfect understanding of the complex PL were overcome by Bourellier et al. [108] via imaging of cathodoluminescence measurements. They have measured a full delocalization of the emitted light through the sample, for emission energies higher than 5.6 eV (blue features in Figure 11), while the emission corresponding to red features on the spectrum is strongly inhomogeneous within individual few layer flakes, with additional emission bands localized at structural departures from crystal perfection, such as faceted plane folds or possible local changes of the hBN layers stacking order. Unfortunately, as the experimental set up of reference [108] was operating from room temperature to at about 150 K, some of the features that are shown in Figure 11 at 5.56 and 5.3 eV are smeared out and thus are not resolved. Photoluminescence experiments conducted at different temperatures show finer structures for temperatures below 50 K [23, 41, 107, 108].

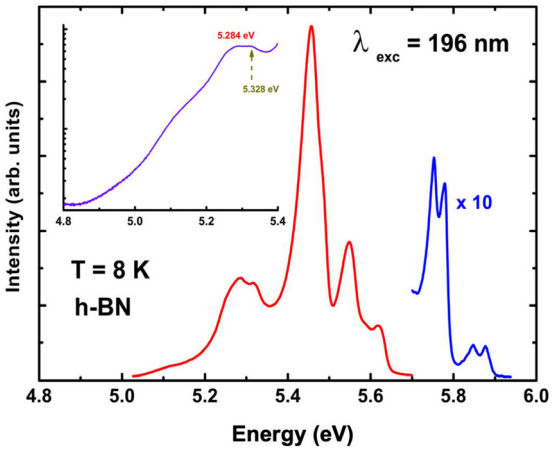

Figure 11: Low temperature photoluminescence spectrum of BN plotted in the 4.8–6.0 eV range. Blue plot: phonon-assisted transitions, red plot phonon assisted overtones recombinations to stacking faults and a PL bands at 5.55 and 5.3 eV. Insert: the 5.3 eV region showing the composite nature with a broad line and the lowest energy of the overtones recombinations to stacking faults.

The situation is rather complicated and its interpretation is the following:

- The high-energy transitions are phonon replicas of a very tiny forbidden indirect excitonic recombination at 5.955 eV. Phonon replicas in hBN involve phonons in the middle of the Brillouin zone as can be seen in Figure 12**.** These radiative recombinations obey selection rules in agreement with predictions of group-theory [23, 41]. This was not straightforward to understand as its roots reside in the non-common nature of the band structure of hBN with the minimum of the conduction sitting at the **M** point of the Brillouin zone and the maximum of the valence band occurring in the neighbourhood of **K** [42, 45]. The radiative recombination of an electron–hole pair under Coulomb interaction requires a phonon of ad-hoc wavevector to satisfy the **k**-selection rule. The situation while being similar to silicon or germanium, or diamond, or GaP, or AlP or AlAs, … is different in the sense that both extrema sit at edges of the Brillouin zone. Instead of needing a phonon at the edge of the Brillouin zone, a phonon at its middle (the so-called T point) along the **Γ-K** direction is needed, according to group-theory considerations [41, 45, 23]. If recording the photoluminescence signal under conditions where the Poynting vector of the emitted photon is collinear to the c axis, phonon at T point having the TA, LA, TO and LO symmetry are required to ensure non vanishing value of the Fermi's golden rule. If performing the photoluminescence experiment under conditions where the Poynting vector of the emitted photon is orthogonal to the c axis, phonon at T point having the ZO_1, ZO_2 symmetries are required to ensure non vanishing value of the Fermi Golden rule. Phonon ZA (A_{2u}) is forbidden and phonon ZO_3 is silent.
- These different phonon replicas all exhibit a fine structure with a series of complementary satellite lines split from each other by 6.8 meV. Their intensity decreases when increasing the overtone index as can be seen in Figure 13**.** This splitting is due to complementary electronic Raman scatterings made possible after the first phonon emission (at T point) and the fulfilment of the **k**-selection rule. These higher order processes involve the low energy Raman active mode at zone centre [109]. Interestingly, the full fitting of the photoluminescence spectrum can be achieved through the whole series of features using Gaussian functions broadened proportionally to the group velocity of the TA, LA, TO, LO phonons at T point. The need of using Gaussian rather than Lorentzian functions and the efficiency of the overtoning was interpreted in terms of the existence of unusually strong exciton–phonon interaction in hBN [43, 44].

At lower energy the photoluminescence spectra of hBN present a series of lines that are also phonon-assisted transitions, but are specific overtones of the initial phonon cascade from the indirect exciton. The first overtone of the series is observed at 5.62 eV. It is followed by a series of 148 meV-split global repeats of the fine structure splitting observed at the scale of the four different phonon replicas TA, LA, TO and LO, which we discussed above. The number

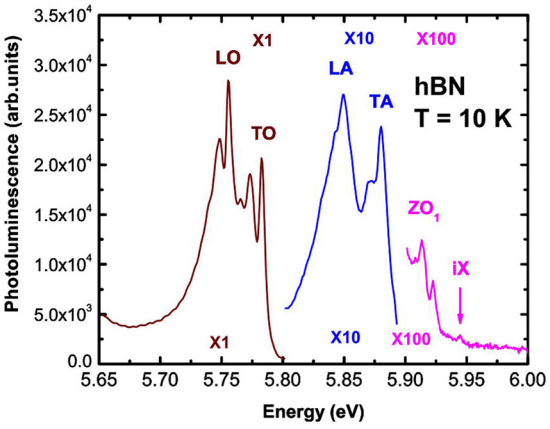

Figure 12: Zoom of the 8 K PL in the 5.65–6.0 eV region to evidence: The signature of the forbidden indirect exciton iX. The phonon assisted series involving ZO_1 (forbidden in the experimental configuration, therefore very weak see ref. [32]); TA, LA TO, LO replicas. At lower energy of each one phonon replica ZO_1, TA, LA TO, LO the series of overtones involving low frequency Raman active mode.

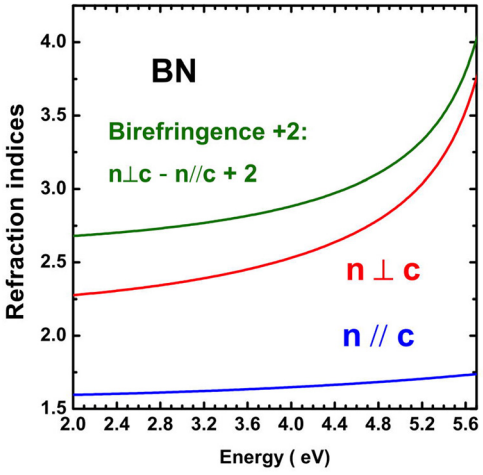

Figure 13: Plot of the in-plane (red) and out-of-plane (blue) refractive index as a function of energy showing the giant natural anisotropy (green) of hBN. The plot of giant natural anisotropy of hBN has been shifted by 2. The parameters used for the plot were taken from reference [22].

of defects that give the final density of states in Fermi's golden rule gives the intensity of the photoluminescence in this energy range, and it can be inhibited in regions free from defects [106, 110]. Defects are appropriately selected by **K-K′** intervalley scattering of carriers in hand and by emission of zone-edge TO(**K**) optical phonons, which is a selection rule process dictated by group theory arguments [111]. Intervalley scattering can be observed till 5.328 eV where it overlaps with a gaussian broad band at 5.284 eV and a full width at half maximum of 83 ± 6 meV. Over the series, there is another band peaking at 5.56 eV and a full width at half maximum of 27 ± 3 meV. These bands were not clearly seen in ref. [108] as they are not so robust with T compared to the other ones and it has been argued that they are probably associated to lattice vacancies or incorporation of atoms in antisite positions [53, 112].

The important result here is the uncommon importance of the electron-phonon interaction in hBN for which the photoluminescence intensity is ruled by interaction of the photo-created carriers with the phonon fields. From a theoretical point of view, such interaction is very hard to describe rigorously and this leads to many difficulties in reproducing all the PL features.

The effects of the electron-phonon interaction in the optical properties can be summarized as: i) a shift in the energy of the optical transitions as a function of temperature due to the band structure renormalization, ii) a broadening of the absorption peaks due to the finite lifetime of the electronic states, and iii) the possibility to observe phonon-assisted recombinations. This is further complicated by the fact that when electron and hole are bound together to form an exciton, the calculation can no longer be limited to independent scatterings between electrons/holes and phonons, which by itself is a not quite a trivial task [113], but it is necessary to evaluate the exciton–phonon interactions. Starting from the pioneering work of Toyozawa [44] and motivated by the presence of always new fascinating and intriguing experimental results, the theoretical community has tried, at different levels of approximations, to fill in the gap of addressing the exciton–phonon coupling [114–117]. The most sophisticated treatment would require the inclusion in the exciton–phonon coupling of what are called the "dynamical effects", which allow to relate to the temperature dependence of the optical transitions and their linewidths/relaxation times. Unfortunately, the most complete treatment proposed up to now [118] is so computationally demanding that it has not been tested on real materials yet. Nevertheless, the theoretical community has attempted to study the hBN photoluminesce in order to corroborate and further elucidate the physical picture at the basis of the PL lines. In a first attempt, the indirect nature of the lowest energy excitons and their binding energy values have been obtained by Schué et al. [46] without including any electron–phonon coupling contributions, from the solution of momentum-dependent Bethe Salpeter Equation (BSE), just to confirm the stability of the observed luminescence intensity and the presence of a direct exciton at a slightly higher energy. In more sophisticated theoretical studies, the PL spectra have been reproduced via the perturbative inclusion of electron–phonon coupling in the BSE by Cannuccia et al. [47] or with the inclusion of exciton–phonon coupling via a finite-difference scheme by Paleari et al. [48], arriving to explaining the structure of the emission spectrum in terms of the two lowest excitons found at the specific finite-**q** (**Γ-T**) coupled with different strengths to the in-plane phonon modes. Those states, observed below the lowest-bound direct exciton, originate from the splitting, at finite momentum, of the doubly degenerate E_{2g} exciton (lowest exciton at $\mathbf{q} = \mathbf{0}$) and, even being dark, can be replicated by the different phonon modes (TA, LA, TO and LO) and acquire a finite optical weight as in Figure 12. Unfortunately, to limit the computational cost, *ad hoc* approximations were used, which limited the overall agreement with the experiments, reduced the predictive power of the approaches and prevented building a complete picture of the complex underlying physics.

Efforts have to be pursued in order to interpret more quantitatively within the context of the textbook theory of Toyozawa [44], the square-root dependence against T of the FWHM of the PL [43, 114, 119] (see Figure 14). This very unusual behaviour is expected to have important implications in the area of UV optoelectronics as Schué et al. [45] have measured a huge internal quantum efficient of 50 per cents for the light emission at room temperature. The dipole created by the electron-hole pair polarizes the lattice and the relaxation of the atomic positions is very fast (efficient one-phonon and/or several-phonon emissions) compared to the radiative time and of course nonradiative recombinations. The nonradiative recombination channels are thus by-passed [120].

Advantage can be taken of this performance for DUV LEDs with operating wavelengths smaller than those reachable using conventional nitride, that is to say 235 nm [32]. hBN can be simultaneously used as an efficient material for light emission and a transparent one for light extraction in the context of a simple LED design based on a pn junction. This is at 210 nm, *mutatis mutandis*, a situation similar to the one encountered in the red-amber-yellow when there were no existing quantum well heterostructures [121]. The issue is the doping which

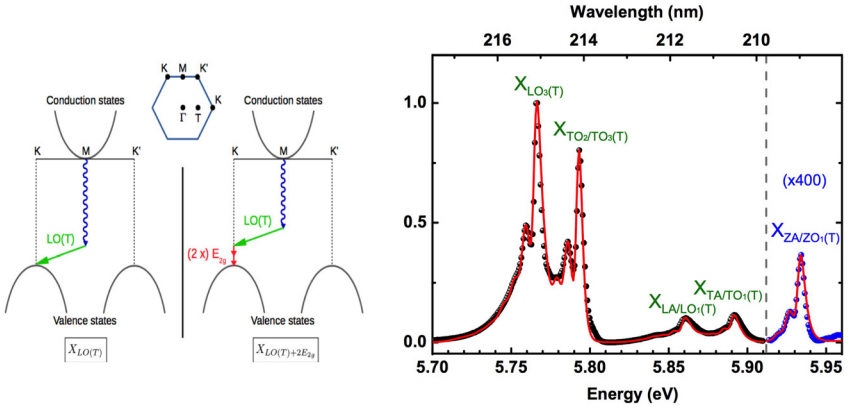

Figure 14: (left) sketch of the scattering mechanism for electronic raman scattering giving birth to the overtoning via the low frequency raman active mode E_{2g}. (right) Full line shape fitting using gaussian functions broadened proportionnaly to the phonon group velocity at the middle of the Brillouin zone.

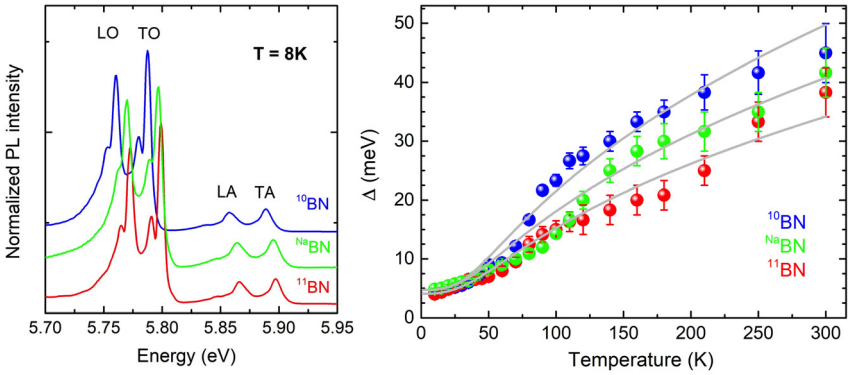

Figure 15: (left) High-energy PL features for BN grown with natural boron ^{Nat}B (green), ^{11}B(red) and ^{10}B(blue) monoisotopically purified boron. Note the redshift with decreasing of the average boron mass, which evidences modifications of the phonon energies over the series of samples. Right: plot of temperature-induced modification of the evolution of the PL line width over the series of samples in correlation with the modification of the energy of ZO_3 (B_{1g}) interlayer silent breathing mode at (fitted values are scaling from 50 ± 10 meV, to 70 ± 10, and then115 ± 10 meV in ^{11}BN, ^{Nat}BN and ^{10}BN, respectively) This figure is a reproduction of figures 2(a) and figure 4(b) in reference [119].

still remains routinely unsolved. One important result is the residual p-type doping of hBN [122], most probably due to native defects [53, 60].

5.2 From epilayers to the monolayer from indirect to direct band gap

A lot of efforts have been dedicated to the epitaxial growth of hBN epilayers and they continue to be. Growth of bulk hBN crystals is realized after solidification of a melt of precursors ([16–18, 123] and refs therein) and their sizes are critically depending on the tricks under the technology used to cool down the melt in order to trigger and control as much as possible its solidification [124]. In epitaxial approaches of the growth, the boron nitride is (with hopefully good stoichiometry) deposited on a target substrate which can be a metal like gold [124], copper [125–127], or sapphire [128, 129] or Highly Ordered Pyrolitic Graphite [40] or the Si face of SiC [130] to cite a few examples. The critical issues are the low growth rate, the need to operate the growth at high temperature, to control the coalescence of here and there germinated hBN nanocrystals [132] … . Efforts have been mainly dedicated to the realization of high-quality monolayers for which the band gap is direct in **K** [40] as reported by comparing the huge oscillator strength measured at the energy of the band gap by reflectivity and its almost vanished stokes-shift with low temperature PL measurements. In general, the photoluminescence of few-monolayer hBN films is dominated by defects like the PL of bulk crystals is. These defects have however different origins: in the case of bulk, they were extensively studied by Bourrellier et al. in [108] and they are attributed to stacking faults whilst in case of epilayers they corresponds to defects at the interfaces of coalesced grains [131]. Using a more spatially focused beam than a laser one, that is to say by doing cathodoluminescence measurements, it is possible to excite regions of the crystal free from defects. Then the fluorescence is freed from contributions of such defects [17, 110, 132]. However, cathodoluminescence measurements failed to detect fluorescence for thicknesses smaller than six monolayers [133]. Shigefusa Chichibu and his researchers of the Tohoku University recently overcame the experimental drawbacks preventing to measure cathodoluminescence signal on thinner samples. Using the monolayer sample grown by Sergey Novikov at

the Nottingham University and used in reference [40], they managed to detect cathodoluminescence signal free from inelastic Raman scattering, thus confirming the interpretation of reference [40, 134].

6 BN and quantum technologies

The high density of defects in hBN combined with the high value of its band gap has triggered the search for defects susceptible to operate as single photon sources (SPS) [56, 61]. A lot of them have been detected in the 4–1.5 eV emission range.

6.1 Defects at 4 eV

In Figure 16 are summarized some PL spectra collected for bulk hBN samples grown under the presence or not of foreign impurities C, Si, Mg. It is worthwhile reminding here that doping of hBN is far from trivial. Nothing specific is observed except the rise of a series of peaks at 4.1 eV when growth conditions depart from using ultra pure B and N precursor. These peaks were initially attributed to carbon incorporation in the lattice [135] but this interpretation is no longer shared [136–143]. It is obvious that it is related to a probable influence of the impurities of the precursors that impact the formation of a perfect crystal or contaminate it. They are in general observed if using an hBN powder [55] but they were never if using B and N and the growth protocol leading to the samples of ref [119]. It has been suggested to attribute these lines to carbon dimers C_BC_N that are expected to form whenever carbon is present during growth, explaining the observed correlation between the presence of carbon and the 4.1 eV line [143]. It is worthwhile noticing that the pressure coefficient of these transitions is smaller than the pressure coefficient of the band gap, which is typical of deep levels [144, 145]. Recently, single-photon emission associated with the 4.1 eV band has been reported [58] using cathodoluminescence excitation while we failed insofar to isolate Single Photon Source in our samples with 4.1 eV emission in far field macroscopic PL experiment, using a laser as an exciting source. We speculate that the larger size of the laser spot compared to the lateral extension of the electron beam used in CL experiments prevents to isolate SPS at 4.1 eV. In fact, as alluded to earlier we have not found any of them neither by macro PL nor by micro PL in samples grown using mono-isotopically purified boron and nitrogen gas as precursors for the growth of hBN, while they are found in macro PL if using BN powders as reported in ref. [55] but are too many for giving isolated centres by micro PL and SPSs could not be isolated. Group theory analysis of the local lattice symmetry in the vicinity of various lattice defects can be found in the paper of Abdu et al. [146]. They introduce the symmetry of the wave functions for neutral and charge defect states and the complementary splitting that may appear under the action of the Jahn–Teller coupling. This paper which is an essential passport for going further into the comprehension of the optical properties of defects giving birth to single photon sources gives the basic tools for the extension of their study to any case not treated in it. Very recently Hamdi et al. have re-examined the interpretation of the nature of the defect at the origin of the 4.1 eV emission [146]. They propose a Stone–Wales defect, a structural defect isovalent to the perfect lattice, based on modification of two adjacent hexagons, formed by a pentagon (passing by atoms we label here e.g. $\mathbf{B_1}$, $\mathbf{B_2}$, N_1, B_3, N_2, and ending to $\mathbf{B_1}$) thus with a boron antisite, coupled to and heptagon (passing by atoms B_1, N_2, B_4, N_3, B_5,$\mathbf{N_4}$, $\mathbf{N_5}$, end closing the curve to $\mathbf{B_1}$) with a nitrogen antisite. The pentagon and the heptagon share the N_2B_1 bond and B_1B_2 and N_4N_5 bonds are formed giving birth to levels 400 meV below the conduction band and 440 meV above the valence band respectively. This is an isoelectronic level with fully occupied ground state and empty upper state, which is therefore electrically and optically active defect. Hamdi et al. [147] argue about the superiority of their model based, on the argument that « the peak positions in the phonon sideband of the 4.1 eV emitter can be well-explained by the (quasi) localized phonon modes associated by the Stone–Wales defect, which should be a unique fingerprint and no other defect produces exactly such a feature ». Based on the observation or not of complementary lines at higher reported in ref. [55], it is clear that complementary investigations both theoretically and experimentally are needed to disentangle the spectroscopic data at these energies. The question of an overlap of both contributions cannot be disregarded at the time of writing.

6.2 Defects at energies below 4 eV

There are a lot of complementary narrow PL lines below 4 eV, some of them being shown in references [58, 61, 148].

A couple of typical examples of emission in the 2 eV region are offered in Figure 17 as well as their $g_2(\tau)$ signals, evidence of anti-bunching that is to say of single photon emissions. Assignment of these lines in term of crystal defect is challenging. By combining direct lattice imaging of hBN with electronic structure calculations,

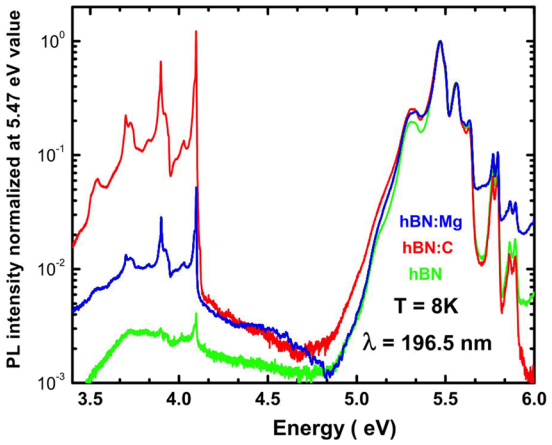

Figure 16: Low temperature photoluminescence spectra of different hBN crystals: undoped hBN from hqgraphene (green); grown under Mg-rich ambient (blue plot, figure 1 of reference [31]) and under moderately C-rich ambient (red plot, spectrum C20 in figure 1 of reference [55]).

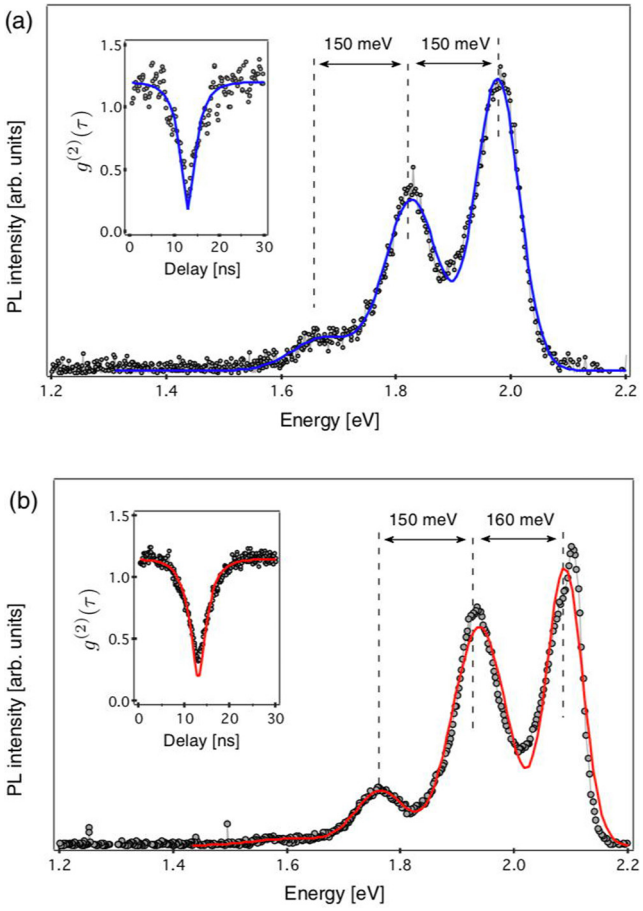

Figure 17: (a), (b) PL spectra recorded from individual defects at 2 eV in hBN at room temperature under green laser illumination. The solid lines are data fitting with Gaussian functions. The insets show the corresponding second-order correlation function $g^{(2)}(\tau)$. After reference [58].

Daichi Kozawa et al. [61] have recently proposed an assignment in terms of various declinations of an up to 16-atom triangular defect around a single B vacancy. According to [60], an optical transition where an electron is excited from a doubly occupied boron dangling bond to a localized B p_z state is expected to give rise to a zero-phonon line of 2.06 eV. This field is very active at the time being both from the experimental and theoretical sides [56–61, 148–157]. Undoubtfully, the quest for a defect with a spin [158] susceptible to challenge the NV centre in diamond [159] or the double vacancy in SiC [160] motivates most of these studies.

We first discuss the PL in the 765 nm range that is to say for energy of 1.62 eV. Based on group theory considerations in D_{3h} symmetry of the ground state, Ivady et al. [161], while computing the fine structure of neutral and charged boron vacancy V_B, found several allowed optical transitions and spin–orbit interactions, that may allow spin dependent nonradiative transitions. The in-plane dangling bonds and the out of plane p_z orbitals of the three neighbour nitrogen atoms give rise to a set of non-degenerate A and degenerate E single particle defect states. The six defect states are occupied with 10 electrons in the negative charge state. Depending whether the in-plane dangling forms the defect state bonds or the out of plane p_z orbitals, they distinguish prime and double prime defect states, respectively. In their notations, the lowest three excited states are $^3A_2''$ $^3E''$, and $^3E'$ in the triplet manifold and the three lowest excited states are $^1E'$, $^1A_2''$, and $^1E''$, in the singlet manifold. As obtained from *ab initio* simulations, the photoluminescence spectrum at 765 nm at 300 K (1.62 eV) is attributed to the zero phonon line for the $^3E'' \rightarrow {}^3A_2'$ transition computed at 1.71 eV and the 1.318 eV to the $^1E'' \rightarrow {}^1E_2'$. To this V_B is associated a very rich hyper-fine structure splitting resulting in a spectroscopy including a polarization-dependent optical response extensively described in their paper and which details are for experts of the field and fall out of the scope of the present review. However, investigations of hyperfine structure splittings and spin-related phenomena are currently under the go [162] although being very challenging. Recently, also Mendelson et al. [163] focused experimentally on the emission at 585 nm (2.1 eV) that they suggest defects such as N_BV_N and C_BV_N to be potential candidates. Light emitted by such defects is varying through the 573–650 nm range and it is sensitive to an apply strain field or to the amount of carbon incorporated during the growth [164].

Going one step further in terms of theoretical understanding, Li et al. address the V_NN_B colour centres under strain [165]. It is known that these defects initially proposed

to emit at 630 nm [56] can emit light over the 569–697 nm range and that emission diagram displays a distribution of orientations [166–172]. The paper by Li et al. [166] is difficult, but, well written, and particularly interesting as it shows that local strain field can as well modify the energy spectrum as the overall set of the optical properties of the V_NN_B colour centres over a large range of wavelengths.

Hayee et al. [172] argue based on their own experiments and theoretical papers [54, 173] that interstitial carbon and oxygen should be considered in addition to the consideration of the contribution of native defects, as an evidence of the difficulty to meet a general consensus at the light of the existing measurements and calculations for defects emitting below 4 eV.

6.3 Next (challenging) experiments

Most of the optical experiments have been carried out, the Poynting vector of the exciting and collected photons being collinear or almost collinear to the high symmetry axis of hBN, that is to say with Poynting vector orthogonal to the reticular plane (0001). Using an alternative configuration with the Poynting vector parallel to this reticular plane, optical signatures of ZO phonons could be evidenced to contribute to the PL in the 6 eV region [23].

Several theoretical papers dedicated to Mg doping or defects operating either at 2 or 4 eV have predicted a possible displacement of atoms or formation of dangling bonds away from the (0001) plane, which is a situation that can give birth to a dipole away from this (0001) plane. Among them are the papers dedicated to the polaron effect in BN: Mg, [54], the dangling bonds invoked for explaining the 2.06 eV recombination [61], the C_BC_N dimers as potential candidates triggering the 4 eV recombination [147], the V_NN_B defect with ground state of C_{1h} symmetry and one of its excited states of C_{2V} symmetry [165]. Of course such dipole is weak or it vanishes. But we believe that measuring the emission diagrams of such defects, which Chris van de Walle and his colleague explicitly ask for, will boost the understanding to unexplored degrees [142]. Of course it is difficult but science is not exciting if not challenging. At the time of writing, there still remains a lot of work to be done before there is a consensual final and robust identification of the « what gives what ».

The long time required to understand subtle phenomena should not be a surprise: the physics of nitrogen in the (Ga, In, Al) (AsP) alloys is the best example one could exhume here to plead for the need of ad-hoc ripening time. Nitrogen as a single impurity (isoelectronic substituent of the anion) or paired or in triplet assemblies, first discovered and not identified as it in the group of Gross in about 1962 [174], has been extensively used for the realization of red to yellow light emitting diodes [175] before the utilization of quantum wells. Although identified as the ad-hoc impurity for green-yellow emission by David Thomas and John J. Hopfield [176], its physics was not fully elucidated before the works of Paul Richard Charles Kent in the team of Alex Zunger at the dawn of the 21st century [177], after hundreds of publications were dedicated to its investigation and to the understanding of its interaction with the electronic states of its host crystals.

7 Conclusions

Without the need to conceive and to realize compact solid state light emitters that operate in the deep ultraviolet for large scale killings of bacteria and viruses with portable and convenient devices, at operation wavelengths shorter than accessible by the AlN-based technology [178], the deep UV emitter published by Watanabe and Taniguchi in 2004 and 2009 [16, 19] might not have attracted researchers and hBN should probably not have buzzed. However, the second birth of the 2D materials, also at the dawn of the current century and the need to cap them, for taking advantage of their nice light–matter coupling efficiency, combined with their crystalline compatibility with the layered structure of hBN, another 2D material, boosted it under the limelight of modern information technology [179]. The lack of intense studies regarding its growth under very difficult conditions (it melts at 2950 °C) has offered us a material with quite many lattice defects, many of them being efficient single photon sources. Maybe that the main player in the arena theatre where will be played quantum information technologies will be that old guy, born in 1842, but now often presented as a new comer. Who knows? Russians say «новое часто старое, хорошо забытое»: the novelty is often a well-forgotten oldie.

Acknowledgments: This work was financially supported in France by the contract BONASPES (ANR-19-CE30-0007-02) under the umbrella of the publicly funded Investissements d'Avenir program managed by the French ANR agency. This work has been supported in Spain the Spanish MINECO/FEDER under Contracts No. MAT2015-71035-R and No. MAT2016-75586-C4-1-P. We are grateful to Anais Dréau, James H. Edgar, Christine Elias, Adam Gali, Ryota Ishii, Vincent Jacques, Rafael J. Jiménez-Riobóo, Matthieu Kociak, Christian L'Hénoret, Jiahan Li, Song Liu, Thierry Michel, Sergey V. Novikov, Ryan Page, Thomas Pelini,

Isabelle Philip, Alfredo Segura, Odile Stefan, Takashi Taniguchi, Luiz H.G. Tizei, Pierre Valvin, Chris G. van de Walle, Arie van der Lee, Thi Quynh Phuong Vuong, Nikolay D. Zighadlo, Alberto Zobelli and many others. BG acknowledges support of Dr. Eng. Dennis Couwenberg, Publishing Editor of Nanophotonics for suggesting the writing of this review.

Author contributions: All the authors have accepted responsibility for the entire content of this submitted manuscript and approved submission.

Research funding: None declared.

Conflict of interest statement: The authors declare no conflicts of interest regarding this article.

References

[1] W. H. Balmain, "XLVI. Observations on the formation of compounds of boron and silicon with nitrogen and certain metals," *J. Prak. Chem.*, vol. 27, pp. 422–430, 1842.

[2] B. Archibald, "Catalogue of Minerals found in the interior of the State of New York," *Am. Mineral. J.*, vol. 1, pp. 96–97, 1810.

[3] J. Brooke, and A. Der Connell, "Greenockit, ein neues Mineral," *Ann. Phys. Chem.*, vol. 127, pp. 274–276, 1840.

[4] A. Magnus, and H. Danz, "Die spezifische Wärme von Wolfram, Bor, Borstickstoff und Berylliumoxyd," *Ann. Phys.*, vol. 386, pp. 407–424, 1926.

[5] A. Simpson, and A. D. Stukes, "The thermal conductivity of highly oriented pyrolitic boron nitride," *J. Phys. C: Solid State Phys.*, vol. 4, pp. 1710–1718, 1971. and references therein.

[6] E. K. Sichel, R. E. Miller, M. S. Abrahams, and C. J. Buiocchi, "Heat capacity and thermal conductivity of hexagonal pyrolitic boron nitride," *Phys. Rev. B*, vol. 13, pp. 4607–4611, 1976.

[7] B. Mortazavi, Luiz Pereira, C. Felipe, Jiang Jin-Wu, and T. Rabczuk, "Modelling heat conduction in polycrystalline hexagonal boron nitride films," *Sci. Rep.*, vol. 5, pp. 13228, 2015.

[8] Z. Zhang, S. Hu, J. Chen, and B. Li, "Hexagonal boron nitride:a promising substrate for graphene with high heat dissipation," *Nanotechnology*, vol. 28, pp. 225704, 2017.

[9] L. Lindsay, and D. A. Broido, "Enhanced thermal conductivity and isotope effect in single layer hexagonal boron nitride," *Phys. Rev. B*, vol. 84, pp. 155421–155425, 2011.

[10] P. Jiang, X. Qian, R. Yang, and L. Lindsay, "Anisotropic thermal transport in bulk hexagonal boron nitride," *Phys. Rev. Mater.*, vol. 2, 2018, Art no. 064005.

[11] Q. Cai, D. Scullion, W. Gan, et al., "High thermal conductivity of high-quality monolayer boron nitride and its thermal expansion," *Sci. Adv.*, vol. 5, 2019, eaav0129.

[12] V. Sharmaa, H. L. Kagdada, P. K. Jha, P. Śpiewak, and J. Kurzydłowski, "Thermal transport properties of boron nitride based materials:a review," *Renew. Sust. Energy Rev.*, vol. 120, p.109622, 2020.

[13] https://en.wikipedia.org/wiki/Walther_Bothe.

[14] https://en.wikipedia.org/wiki/James_Chadwick.

[15] M. Henske, M. Klein, M. Köhli, et al., "The 10B-based jalousie neutron detector," *Nucl. Instrum. Methods. Phys. Res. A.*, vol. 686, pp. 151–155, 2012.

[16] K. Watanabe, T. Taniguchi, and H. Kanda, "Direct-bandgap properties and evidence for ultraviolet lasing of hexagonal boron nitride single crystal," *Nat. Mat.*, vol. 3, pp. 404–409, 2004.

[17] S. Song Liu, R. He, and Z. Ye, et al., "Large-scale growth of high-quality hexagonal boron nitride crystals at atmospheric pressure from an Fe–Cr flux," *Cryst. Growth Des.*, vol. 17, pp. 4932–4935, 2017.

[18] N. D. Zhigadlo, "Crystal growth of hexagonal boron nitride (hBN) from Mg–B–N solvent system under high pressure," *J. Cryst. Growth*, vol. 402, pp. 308–311, 2014.

[19] K. Watanabe, T. Taniguchi, T. Niiyama, K. Miya, and M. Taniguchi, "Far-ultraviolet plane-emission handheld device based on hexagonal boron nitride," *Nat. Photonics*, vol. 3, pp. 591–594, 2009.

[20] A. Segura, L. Artus, R. Cusco, T. Taniguchi, G. Cassabois, and B. Gil, "Natural optical anisotropy of h-BN: highest giant birefringence in a bulk crystal through the mid-infrared to ultraviolet range," *Phys. Rev. Mater.*, vol. 2, 2018, 024001.

[21] R. J. Jimenez-Riobo, L. Artus, R. Cusco, T. Taniguchi, G. Cassabois, and B. Gil, "In-and out-of-plane longitudinal acoustic-wave velocities and elastic moduli in h-BN from Brillouin scattering measurements," *Appl. Phys. Lett.*, vol. 112, 2018, 051905.

[22] A. Segura, R. Cusco, T. Taniguchi, et al., "High-pressure softening of the out-of-plane A_{2u}(transverse-optic) mode of hexagonal boron nitride induced by dynamical buckling," *J. Phys. Chem. C Am. Chem. Soc.*, vol. 123, pp. 17491–17497, 2019.

[23] T. Q. P Vuong, G. Cassabois, P. Valvin, et al., "Phonon symmetries in hexagonal boron nitride probed by incoherent light emission," *2D Mater.*, vol. 4, 2017, 011004.

[24] J. D. Caldwell, A. V. Kretinin, Y Chen, et al., "Sub-diffractional volume-confined polaritons in the natural hyperbolic material hexagonal boron nitride," *Nat. Commun.*, vol. 5, p. 5221, 2014.

[25] J. D. Caldwell, I. Aharonovich, G. Cassabois, J. H. Edgar, B. Gil, and D. N. Basov, "Photonics with hexagonal boron nitride," *Nat. Rev. Mater.*, vol. 4, pp. 552–567, 2019.

[26] A. Poddubny, I. Iorsh, P. Belov, and Y. Yuri Kivshar, "Hyperbolic Metamaterials," *Nat. Photonics*, vol. 7, pp. 948–957, 2013.

[27] D. N. Basov, M. M. Fogler, and F. J. Garcia de Abajo, "Polaritons in van der Waals materials," *Science*, vol. 354, p. aag1992, 2017.

[28] N. Kinsey, C. DeVault, A. Boltasseva, and V. M. Shalaev, "Near-zero-index materials for photonics," *Nat. Rev. Mater.*, vol. 4, pp. 742–760, 2019.

[29] Y. Kobayashi, K. Kumakura, T. Akasaka, and T. Makimoto, "Layered boron nitride as a release layer for mechanical transfer of GaN-based devices," *Nature*, vol. 484, p. 223, 2012.

[30] F. Cadiz, E. Courtade, C. Robert, et al., *Phys. Rev. X*, vol. 7, 2017, 021026. and references therein.

[31] A. C. Gomez, "Why all the fuss about 2D semiconductors?," *Nat. Photonics*, vol. 10, pp. 202–204, 2016.

[32] A. A. Toropov, E. A. Evropeitsev, M. O. Nestoklon, et al., "Strongly confined excitons in GaN/AlN nanostructures with atomically thin GaN layers for efficient light emission in deep-ultraviolet," *Nano Lett.*, vol. 20, pp. 158–165, 2020.

[33] Michael Kneissl, and Jens Rass, editors. *III-Nitride Ultraviolet Emitters:Technology and Applications*. *Springer Series in Materials Science*. Springer International Publishing, 2016.

[34] Z. Zhang, M. Kushimoto, T. Sakai, et al., "A 271.8 nm deep-ultraviolet laser diode for room temperature operation," *Appl. Phys. Express*, vol. 12, p. 124003, 2019.

[35] A. Rodger *UV Absorbance Spectroscopy of Biological Macromolecules-in Encyclopedia of Biophysics -Gordon C*. K. Roberts Ed. Heidelberg, New York Dordrecht London, Springer, 2013, pp. 2714–2718. https://doi.org/10.1007/978-3-642-16712-6.
[36] M. Zastrow, "Meet the crystal growers who sparked a revolution in graphene electronics," *Nature*, vol. 572, pp. 429–432, 2019.
[37] R. Dahal, J. Li, S. Majety, et al., "Epitaxially grown semiconducting hexagonal boron nitride as a deep ultraviolet photonic material," *Appl. Phys. Lett.*, vol. 98, p. 211110, 2011.
[38] T.S. Cheng, A. Davies, A. Summerfield, et al., "High temperature MBE of graphene on sapphire and hexagonal boron nitride flakes on sapphireJournal of Vacuum," *Sci. Technol. B.*, vol. 34, 2016, 02L101.
[39] R. Page, J. Casamento, Y. J. Cho, et al., "Rotationally aligned hexagonal boron nitride on sapphire by high-temperature molecular beam epitaxy," *Phys. Rev. Mater.*, vol. 3, 2019, 064001.
[40] C. Elias, P. Valvin, T. Pelini, et al., "Direct band-gap crossover in epitaxial monolayer boron nitride," *Nat. Commun.*, vol. 10, p. 2639, 2019.
[41] G. Cassabois, P. Pierre Valvin, and B. Gil, "Hexagonal boron nitride is an indirect band gap semiconductor," *Nat. Photonics*, vol. 10, p. 262, 2016.
[42] B. Arnaud, S. Lebegue, P. Rabiller, and M. Alouani, "Huge excitonic effects in layered hexagonal boron nitride," *Phys. Rev. Lett.*, vol. 96, 2006, 026402.
[43] T. Q. P. Vuong, G. Cassabois, P. Valvin, S. Liu, J. H. Edgar, and B. Gil, "Exciton-phonon interaction in the strong-coupling regime in hexagonal boron nitride," *Phys. Rev. B*, vol. 95, 2017, 201202.
[44] Y. Toyozawa, "Theory of line-shapes of the exciton absorption bands," *Prog. Theor. Phys.*, vol. 20, pp. 53–81, 1958.
[45] G. Fugallo, M. Aramini, and J. Koskelo, "Exciton energy-momentum map of hexagonal boron nitride," *Phys. Rev. B*, vol. 92, 2015, 165122.
[46] L. Schué, L. Sponza, A. Plaud, et al., "Bright luminescence from indirect and strongly bound excitons in h-BN," *Phys. Rev. Lett.*, vol. 122, 2019, 067401.
[47] E. Cannuccia, B. Monserrat, and C. Attaccalite, "Theory of phonon-assisted luminescence in solids: application to hexagonal boron nitride," *Phys. Rev. B*, vol. 99, 2019, 081109.
[48] F. Paleari, H. P. C. Miranda, A. Molina-Sánchez, and L. Wirtz, "Exciton-phonon coupling in the ultraviolet absorption and emission spectra of bulk hexagonal boron nitride," *Phys. Rev. Lett.*, vol. 122, 2019, 187401.
[49] T. Galvani, F. Paleari, H. P. C. Miranda, et al., "Angular resolved electron energy loss spectroscopy inhexagonal boron nitride," *Phys. Rev. B*, vol. 94, 2016, 125303.
[50] P. Cudazzo, L. Sponza, C. Giorgetti, L. Reining, F. Sottile, and M. Gatti, "Exciton band structure in two-dimensional materials," *Phys. Rev. Lett.*, vol. 116, 2016, 066803.
[51] J. Koskelo, G. Fugallo, M. Hakala, M. Gatti, F. Sottile, and P. Cudazzo, "Excitons in van der Waals materials: from monolayer to bulk hexagonal boron nitride," *Phys. Rev. B*, vol. 95, 2017, 035125.
[52] L. Sponza, H. Amara, F. Ducastelle, A. Loiseau, and C. Attaccalite, "Exciton interference in hexagonal boron nitride," *Phys. Rev. B*, vol. 97, no. 2018, 2018, 075121.
[53] L. Sponza, H. Amara, C. Attaccalite, et al., "Direct and indirect excitons in boron nitride polymorphs:a story of atomic configuration and electronic correlation," *Phys. Rev. B*, vol. 98, p. 125206, 2018.
[54] L. Weston, D. Wickramaratne, M. Mackoit, A. Alkauskas, and C. G. Van de Walle, "Native point defects and impurities in hexagonal boron nitride," *Phys. Rev. B*, vol. 97, p. 214104, 2018. and references therein.
[55] T. Pelini, C. Elias, R. Page, L. Xu, S. Liu, J. Li, et al., "Shallow and deep levels in carbon-doped hexagonal boron nitride crystals," *Phys. Rev. Mater.*, vol. 3, 2019, 094001.
[56] A. Bommer, and Becher, "New insights into nonclassical light emission from defects in multi-layer hexagonal boron nitride," *Nanophotonics*, vol. 8, pp. 2041–2048, 2019.
[57] T. T. Tran, K. Bray, M. J. Ford, M. Toth, and I. Aharonovich, "Quantum emission from hexagonal boron nitride monolayers," *Nat. Nanotechnol.*, vol. 11, pp. 37–41, 2016.
[58] L. J. Martinez, T. Pelini, V. Waselowski, et al., "Efficient single photon emission from a high-purity hexagonal boron nitride crystal," *Phys. Rev. B*, vol. 94, p. 121405, 2016.
[59] R. Bourrellier, S. Meuret, A. Tararan, et al., "Bright UV single photon emission at point defects in h-BN," *Nano Lett.*, vol. 16, pp. 4317–4321, 2016.
[60] N. V. Proscia, R. J. Collison, C. A. Meriles, and V. M. Menon, "Coupling of determiniscally activated quantum emitters in hexagonal boron nitrile to plasmonic surface lattice resonances," *Nanophotonics*, vol. 8, no. 11, pp. 2057–2064, 2019.
[61] M. E. Turiansky, A. Alkauskas, L. C. Bassett, and C. G. Van de Walle, "Dangling bonds in hexagonal boron nitride as single-photon emitters," *Phys. Rev. Lett.*, vol. 123, p. 127401, 2019.
[62] D.Kozawa, A. G.Rajan, S. X.Sylvia Xin Li, et al., *Observation and Spectral Assignment of a Family of Hexagonal Boron Nitride Lattice Defects*. https://arxiv.org/pdf/1909.11738.pdf.
[63] R. S. Pease, "Crystal structure of boron nitride," *Nature*, vol. 165, p. 722, 1950.
[64] R. S. Pease, "An X-ray study of boron nitride," *Acta. Crystallogr.*, vol. 5, pp. 356–361, 1952.
[65] S. M. Gilbert, T. Pham, M. Dogan, et al., "Alternative stacking sequences in hexagonal boron nitride," *2D Mater.*, vol. 6, 021006, 2019.
[66] R. M. Ribeiro, and N. M. R. Peres, "Stability of boron nitride bilayers:ground-state energies, interlayer distances, and tight-binding description," *Phys. Rev. B*, vol. 83, p. 235312, 2011.
[67] G. Constantinescu, A. Kuc, and T. Heine, "Stacking in bulk and bilayer hexagonal boron nitride," *Phys. Rev. Lett.*, vol. 111, 036104, 2013.
[68] J. F. Nye, *Physical Properties of Crystals: Their Representation by Tensors and Matrices*, Oxford, Oxford University Press, 1957, 978-0-19-851165-6.
[69] P. Ares, T. Cea, M. Holwill, et al., "Piezoelectricity in monolayer hexagonal boron nitride," *Adv. Mater.*, vol. 32, p. 1905504, 2020.
[70] G. Wang, A. Chernikov, M. M. Glazov, et al., "Excitons in atomically thin transition metal dichalcogenides," *Rev. Mod. Phys.*, vol. 90, 2018, 021001.
[71] F. George, *Koster in "Properties of the thirty-two point groups" M.I*, Cambridge, MA, T. Press, 1963.
[72] H. Poulet, and J. P. Mathieu, *Vibration Spectra and Symmetry of Crystals*, New York, London Paris, Gordon and Breach, 1976.
[73] E. Doni, and G. Pastori Parravicini, "Energy bands and optical properties of hexagonal boron nitride and graphite," *Il Nuovo Cimento B*, vol. 64, pp. 117–144, 1969.

[74] R. Geick, C. H. Perry, and G. Rupprecht, "Normal modes in hexagonal boron nitride," *Phys. Rev.*, vol. 146, pp. 543–547, 1966.
[75] I. L. Babich, "Raman spectrum of hexagonal boron nitride," *Theor. Exp. Chem.*, vol. 8, pp. 594–595, 1974.
[76] T. Kuzuba, K. Era, T. Ishii, and T. Sato, "A low frequency Raman-active vibration of hexagonal boron nitride," *Solid State Commun.*, vol. 25, pp. 863–865, 1978.
[77] T. Kuzuba, Y. Sato, S. Yamaoka, and K. Era, "Raman-scattering study of high-pressure effects on the anisotropy of force constants of hexagonal boron nitride," *Phys. Rev. B*, vol. 18, pp. 4440–4443, 1978.
[78] R. J. Nemanich, S. A. Solin, and R. M. Martin, "Light scattering study of boron nitride microcrystals," *Phys. Rev. B*, vol. 23, pp. 6348–6356, 1981.
[79] D. M. Hoffman, G. L. Doll, and P. C. Eklund, "Optical properties of pyrolytic boron nitride in the energy range 0.05–10 eV," *Phys. Rev. B*, vol. 30, pp. 6051–6056, 1984.
[80] C. L. Cortes, W. Newman, S. Molesky and Z. Jacob, "Quantum nanophotonics using hyperbolic metamaterials hyperbolic phonon polaritons," *J. Opt.*, vol. 14:0630012, 2012. corrigendum:J.Opt. 20143;16:129501.
[81] Z. Jacob, "Hyperbolic phonon polaritons," *Nat. Mater.*, vol. 13, p. 1081, 2014.
[82] A. J. Giles, S. Dai, I. Vurgaftman, et al., "Ultra-low-loss polaritons in isotopically pure materials," *Nat. Mater.*, vol. 17, pp. 134–139, 2018.
[83] Y. Jia, H. Zhao, Q. Guo, X. Wang, H. Wang, and F. Xia, "Tunable plasmon–phonon polaritons in layered graphene–hexagonal boron nitride heterostructures," *ACS Photonics*, vol. 2, pp. 907–912, 2015.
[84] V.L. Solozhenko, G. Will, and F. Elf, "Isothermal compression of hexagonal graphite-like boron nitride up to 12," *GPa Solid State Commun.*, vol. 96, pp. 1–3, 1995.
[85] G. Kern, G. Kresse, and J. Hafner, "Ab initio calculation of the lattice dynamics and phase diagram of boron nitride," *Phys. Rev. B*, vol. 59, p. 8551, 1999.
[86] N. Mounet, and N. Marzari, "First-principles determination of the structural, vibrational and thermodynamic properties of diamond, graphite, and derivatives," *Phys. Rev. B*, vol. 71, p. 205214, 2005.
[87] J. Serrano, A. Bosak, R. Arenal, et al., "Wirtz vibrational properties of hexagonal boron nitride: inelastic X-ray scattering and ab initio calculations," *Phys. Rev. Lett.*, vol. 98, 2007, 095503.
[88] N. Ohba, K. Miwa, N. Naoyuki Nagasako, and A. Fukumoto, "First-principles study on structural, dielectric, and dynamical properties for three BN polytypes," *Phys. Rev. B*, vol. 63, 2001, 115207. Erratum Phys. Rev. B 2008; 77: 129901.
[89] K. H. Michel, and B. Verberck, "Theory of elastic and piezoelectric effects in two-dimensional hexagonal boron nitride," *Phys. Rev. B*, vol. 80, p. 22430, 2009.
[90] K. H. Michel, and B. Verberck, "Phonon dispersions and piezoelectricity in bulk and multilayers of hexagonal boron nitride," *Phys. Rev. B*, vol. 83, p. 115328, 2011.
[91] K. H. Michel, and B. Verberck, "Theory of rigid-plane phonon modes in layered crystals," *Phys. Rev. B*, vol. 85, 2012, 094303.
[92] R. Cuscó, B. Gil, G. Cassabois, and L. Artús, "Temperature dependence of Raman-active phonons and anharmonic interactions in layered hexagonal BN," *Phys. Rev. B*, vol. 94, 2016, 155435.
[93] The quartic anharmonicity channel involves the decay into a zone center phonon and a pair of opposite wave-vector phonons see equation 10 of ref. [92].
[94] D. Zhao, X. Qian, X. Gu, S. A. Jajja and R. R. Yang, "Measurement techniques for thermal conductivity and interfacial thermal conductance of bulk and thin film materials," *J. Electron. Packag.*, vol. 138, 2016, 040802.
[95] J. M. Ziman, *Electrons and Phonons: The Theory of Transport Phenomena in Solids*, New York, Clarendon, 1960.
[96] M. Omini, and A. Sparavigna, "Beyond the isotropic-model approximation in the theory of thermal conductivity," *Phys. Rev. B*, vol. 53, pp. 9064–9073, 1996.
[97] G. Fugallo, M. Lazzeri, L. Paulatto, and F. Mauri, "Ab initio variational approach for evaluating lattice thermal conductivity," *Phys. Rev. B*, vol. 88, 2013, 045430.
[98] A. Cepellotti, G. Fugallo, L. Paulatto, M. Lazzeri, F. Mauri, and N. Marzari, "Phonon hydrodynamics in two-dimensional materials," *Nat. Commun.*, vol. 6, p. 6400, 2015.
[99] J. M. Zhang, T. Ruf, M. Cardona, et al., "Raman spectra of isotopic GaN," *Phys. Rev. B*, vol. 56, p. 14399, 1997.
[100] R. Cuscó, L. Artús, J. H. Edgar, S. Liu, G. Cassabois, and B. Gil, "Isotopic effects on phonon anharmonicity in layered van der Waals crystals: isotopically pure hexagonal boron nitride," *Phys. Rev. B*, vol. 97, p. 155435, 2018.
[101] S. D. Baranowski, and A. L. Efros, "Band edge smearing in solid solutions," *Sov. Phys. Semiconduct.*, vol. 12, pp. 1328–1329, 1978.
[102] equation 8 of ref [91].
[103] D. T. Morelli, J. P. Heremans, and G. A. Slack, "Estimation of the isotope effect on the lattice thermal conductivity of group IV and group III-V semiconductors," *Phys. Rev. B*, vol. 66, 2002, 195304.
[104] M. He, P. Pasqual Rivera, D. Tuan et al., "Valley phonons and exciton complexes in a monolayer semiconductor," *Nat. Commun.*, vol. 11, p. 618, 2020.
[105] S. Brtem, A. Ekman, D. Christiansen, et al., "Phonon-assisted photoluminescence from indirect excitons in monolayers of transition-metal dichalcogenides," *Nano Lett. Article ASAP*, vol. 20, no. 4, pp. 2849–2856.
[106] G. Cassabois, P. Valvin, and B. Gil, "Intervalley scattering in hexagonal boron nitride," *Phys. Rev. B*, vol. 9, 2016, 035207.
[107] K. Watanabe, and T. Taniguchi, "Jahn-Teller effect on exciton states in hexagonal boron nitride single crystal," *Phys. Rev. B*, vol. 79, p. 193104, 2009.
[108] R. Bourrellier, M. Amato, L. H. G. Tizei, et al., "Nanometric resolved luminescence in h-BN flakes:excitons and stacking order," *ACS Photonics*, vol. 1, p. 857, 2014.
[109] T. Q. P. Vuong, G. Cassabois, P. Valvin, et al., "Overtones of interlayer shear modes in the phonon-assisted emission spectrum of hexagonal boron nitride," *Phys. Rev. B* 2017;95: 045207.
[110] K. Watanabe, and T. Taniguchi, "Far-UV photoluminescence microscope for impurity domain in hexagonal-boron-nitride single crystals by high-pressure, high-temperature synthesis," *NPJ 2D Mater. Appl.*, vol. 3, p. 40, 2019.
[111] M. Hulin, "Selection rules for two-phonon absorption processes," *Phys. Status Solidi B*, vol. 21, p. 607, 1967.
[112] C. Attaccalite, M. Bockstedte, A. Marini, A. Rubio, and L. Wirtz, "Coupling of excitons and defect states in boron-nitride nanostructures," *Phys. Rev. B*, vol. 83, no. 2011, p. 144115, 2011.

[113] F. Giustino, "Electron-phonon interactions from first principles," *Rev. Mod. Phys.*, vol. 89, 2017, 015003.
[114] B. Segall, and G. D. Mahan, "Phonon-assisted recombination of free excitons in compound semiconductors," *Phys. Rev.*, vol. 171, pp. 935–948, 1968.
[115] J. Jiang, R. Saito, K. Sato, J. Park, et al., "Exciton-photon, exciton-phonon matrix elements, and resonant Raman intensity of single-wall carbon nanotubes," *Phys. Rev. B*, vol. 75, 2007, 035405.
[116] S. Shree, M. Semina, C. Robert, et al., "Observation of exciton-phonon coupling in MoSe2 monolayers," *Phys. Rev. B*, vol. 98, 2018, 035302.
[117] A Marini, "Ab Initio finite-temperature excitons," *Phys. Rev. Lett.*, vol. 101, p. 106405, 2008.
[118] G.Antonius, and S. G.Louie, *Theory of Exciton Phonon Coupling*. https://arxiv.org/abs/1705.04245.
[119] T. Q. P. Vuong, S. Liu, A. Van der Lee, et al., "Isotope engineering of van der Waals interactions in hexagonal boron nitride," *Nat. Mater.*, vol. 17, p. 152, 2018.
[120] S. Chichibu, Y. Ishikawa, H. Kominami, K. Hara, "Nearly temperature-independent ultraviolet light emission intensity of indirect excitons in hexagonal BN microcrystals," *J. Appl. Phys.*, 123, 2018, 065104.
[121] https://en.wikipedia.org/wiki/Light-emitting_diode.
[122] H. Henck, D. Debora Pierucci, J. Avila, et al., "Direct observation of the band structure in bulk hexagonal boron nitride," *Phys. Rev. B*, vol. 95, 2017, Art no. 085410.
[123] Jiahan Li, Chao Yuan, Christine Elias, et al., "Hexagonal boron nitride single crystal growth from solution with a temperature gradient," *Chem. Mater.*, 2020, (submitted). https://doi.org/10.1021/acs.chemmater.0c00830.
[124] Lee Joo Song, Choi Soo Ho, Yun Seok Joon, et al., "Wafer-scale single-crystal hexagonal boron nitride film via self-collimated grain formation," *Science*, vol. 362, p. 817, 2018.
[125] L. Wang, X. Xu, L. Zhang, et al., "Towards the growth of single crystal boron nitride monolayer on Cu," *Lett. Nat.*, vol. 570, p. 91, 2019.
[126] R. Y. Tay, H. J. Park, G. H. Ryu, et al., "Synthesis of aligned symmetrical multifaceted monolayer hexagonal boron nitride single crystals on resolidified copper," *Nanoscale*, vol. 28, p. 2434, 2016. Also see for an excellent Roland Yingjie Tay in « Chemical Vapor deposition growth and characterization of two-dimensional hexagonal boron nitride », Springer Theses Springer Nature Singapore Pte Ltd 2018.
[127] T. Chen, C. Chuu, C. Tseng, et al., "Wafer-scale single-crystal hexagonal boron nitride monolayers on Cu (111)," *Nature*, vol. 579, pp. 219–223, 2020.
[128] S. Sundaram, X. Li, S. Alam, Y. Halfaya, G. Patriarche, and A. Ougazzaden, "Wafer-scale MOVPE growth and characterization of highly ordered h-BN on patterned sapphire substrates," *J. Cryst. Growth.*, vol. 509, pp. 40–43, 2019.
[129] S. H. Lee, H. Jeong, O. F. N. Okello, et al., "Improvements in structural and optical properties of wafer-scale hexagonal boron nitride film by post-growth annealing," *Sci. Rep.*, vol. 9, p. 10590, 2019.
[130] T. Q. P. Vuong, G. Cassabois, P. Valvin, et al., "Deep ultraviolet emission in hexagonal boronnitride grown by high-temperature molecular beam epitaxy," *2D Mater.*, vol. 4, 2017, 021023.
[131] H. C. Shin, Y. Jang, T. H. Kim, et al., "Epitaxial growth of a single-crystal hybridized boron nitride and graphene layer on a wide-band gap semiconductor," *J. Am. Chem. Soc.*, vol. 137, pp. 6897–6905, 2015.
[132] A. Plaud, L. Schué L., K. K. Watanabe et al. Exciton-exciton annihilation in hBN. *Appl. Phys. Lett.* 2019;114:232103.
[133] L. Schue, B. Berini, B. Placais, et al., "Dimensionality effects on the luminescence properties of hBN," *Nanoscale*, vol. 8, p. 6986, 2016.
[134] S.Chichibu, and K.Shima, *Private Communication*.
[135] A. Katzir, J. T. Suss, A. Zunger, and A. Halperin, "Point defects in hexagonal boron nitride. I. EPR, thermoluminescence, and thermally-stimulated-current measurements," *Phys. Rev. B*, vol. 11, pp. 2370–2377, 1975.
[136] T. Kuzuba, K. Era, T. Ishii, T. Sato, and M. Iwata, "Electron-phonon interactions in layered hexagonal boron nitrile," *Physica B+C*, vol. 105, pp. 339–342, 1981.
[137] T. Taniguchi, and K. Watanabe, "Synthesis of high-purity boron nitride single crystals under high pressure by using Ba–BN solvent," *J. Cryst. Growth.*, vol. 303, pp. 525–529, 2007.
[138] E/. Tsushima, T. Tsujimura, and T. Uchino, "Enhancement of the deep-level emission and its chemical origin in hexagonal boron nitrile," *Appl. Phys. Lett.*, vol. 113, 2018, Art no. 031903.
[139] A. S. Vokhmintsev, I. A. Weinstein, and D. Zamyatin, "Electron-phonon interactions in subband excited photoluminescence of hexagonal boron nitride," *J. Lumin.*, vol. 208, pp. 363–371, 2019.
[140] A. S. Vokhmintsev, I. A. Weinstein, M. G. Minin, and S. A. Shalyakin, "Thermally stimulated processes in the luminescence of carbon-related defects for h-BN micropowder," *Radiat. Meas.*, vol. 124, pp. 35–39, 2019.
[141] T. Korona, and M. Chojecki, "Exploring point defects in hexagonal boron-nitrogen monolayers," *Int. J. Quantum Chem.*, vol. 119, 2019, e25925.
[142] M. Mackoit-Sinkeviciene, M. Maciaszek, C. G. Van de Walle, and A. Alkauskas, "Carbon dimer defect as a source of the 4.1 eV luminescence in hexagonal boron nitrile," *Appl. Phys. Lett.*, vol. 115, p. 212101, 2019.
[143] These lines are not seen by PL in samples grown using mono-isotopically purified boron and nitrogen gas as presursors for the growth of hBN, while they are found if using BN powders as reported in ref.45.
[144] K. Koronski, A. Kaminska, N. D. Zhigadlo, C. Elias, G. Cassabois, and B. Gil, "Spontaneous emission of color centers at 4eV in hexagonal boron nitride under hydrostatic pressure," *Superlattice Microst.*, vol. 131, pp. 1–7, 2019.
[145] Y. Xue, H. Wang, Q. Tan, et al., "Anomalous pressure characteristics of defects in hexagonal boron nitride flakes," *ACS Nano*, vol. 12, pp. 7127–7133, 2018.
[146] M. Abdi, J. P. Chou, A. Gali, and M. B. Plenio, "Color centers in hexagonal boron nitride monolayers:a group theory and ab initio analysis," *ACS Photonics*, vol. 5, p. 1967, 2018.
[147] A.Gali, "Stone-Wales defects in hexagonal boron nitride as ultraviolet emitters," *Private Commun.*
[148] N. R. Jungwirth, B. Calderon, Y. Ji, et al., "Temperature dependence of wavelength selectable zero-phonon emission from single defects in hexagonal boron nitride," *Nano Lett.*, vol. 16, pp. 6052–6057, 2016.
[149] B. Sontheimer, M. Braun, N. Nikolay, et al., "Photodynamics of quantum emitters in hexagonal boron nitride revealed by low-temperature spectroscopy," *Phys. Rev. B*, vol. 96, p. 121202, 2017.

[150] T. T. Tran, M. Kianinia, M. Nguyen, "Resonant excitation of quantum emitters in hexagonal boron nitride," *ACS Photonics*, vol. 5, pp. 295–300, 2018.
[151] A. Dietrich, M. Bürk, E. Steiger, et al., "Observation of Fourier transform limited lines in hexagonal boron nitride," *Phys. Rev. B*, vol. 98, 2018, Art no. 081414.
[152] M. Mehran Kianinia, B. Regan, S. A. Tawfik, et al., "Robust Solid-State Quantum System Operating at 800 K," *ACS Photonics*, vol. 4, pp. 768–773, 2017.
[153] H. Utzat, W. Sun, A. E. K. Kaplan, et al., "Coherent single photon emission from colloidal lead halide perovskite quantum dots," *Science*, vol. 363, pp. 1068–1072, 2019.
[154] G. Grosso, H. Moon, B. Lienhard, et al., "Tunable and high-purity room temperature single-photon emission from atomic defects in hexagonal boron nitride," *Nat. Commun.*, vol. 8, p. 705, 2017.
[155] M. A. Feldman, A. Puretzky, L. Lindsay, et al., "Phonon-induced multicolor correlations in hBN single-photon emitters," *Phys. Rev. B*, vol. 99, 2019, 020101.
[156] K. Konthasinghe, C. Chakraborty, N Mathur et al., "Rabi oscillations and resonance fluorescence from a single hexagonal boron nitride quantum emitter," *Optica*, vol. 6, pp. 542–548, 2019.
[157] B. Spokoyny, H. Utzat, H. Moon, et al., "Effect of spectral diffusion on the coherence properties of a single quantum emitter in hexagonal boron nitride," *J. Phys. Chem. Lett.*, vol. 11, pp. 1330–1335, 2020.
[158] D. D. Awschalom, L. C. Bassett, A. S Dzurak, et al., "Quantum spintronics:engineering and manipulating atom-like spins in semiconductors," *Science*, vol. 339, pp. 1174–1179, 2013.
[159] H. J. Mamin, M. Kim, M. H. Sherwood, et al., "Nanoscale nuclear magnetic resonance with a nitrogen-vacancy spin sensor," *Science*, vol. 339, pp. 557–560, 2013.
[160] D. J. Christle, P. V. Klimov, C. F. de las Casas, et al., "Isolated spin qubits in SiC with a high-fidelity infrared spin-to-photon interface," *Phys. Rev. X*, vol. 7, 2017, Art no. 021046.
[161] V.Ivady, G.Barcza, G.Thiering, et al., *GaliA. Ab initio Theory of Negatively Charged Boron Vacancy Qubit in hBN*. https://arxiv.org/pdf/1910.07767.
[162] N.Chejanovsky, A.Mukherjee, Y.Kim, et al., *J. Single Spin Resonance in a van der Waals Embedded Paramagnetic Defect*. https://arxiv.org/abs/1906.05903.
[163] N.Mendelson, M.Doherty, M.Toth, et al., *Strain Engineering of Quantum Emitters in Hexagonal Boron Nitride*. https://arxiv.org/abs/1911.08072.
[164] N.Mendelson, D.Chugh, T. S.Cheng, et al., *Carbon as the Source of Visible Single Photon Emission from Hexagonal Boron Nitride*. https://arxiv.org/pdf/2003.00949.
[165] S.Li, J. P.Jyh-Pin Chou, A.Hu, et al., *Giant Shift upon Strain on the Fluorescence Spectrum of V_NN_B Color Centers in h-BN*. https://arxiv.org/pdf/2001.02749.
[166] N.Chejanovsky, M.Rezai, F.Paolucci, et al., *Structural Attributes and Photo-dynamics of Visible Spectrum Quantum Emitters in Hexagonal Boron Nitride*. https://arxiv.org/pdf/1608.03114.
[167] T. T. Tran, C. Elbadawi, D. Totonjian, et al., "Robust multicolor single photon emission from point defects in hexagonal boron nitrile," *ACS Nano*, vol. 10, pp. 7331–7338, 2016.
[168] C. L. Zai, Z. Q. Xu, N. Mendelson, M. Kianinia, et al., "Purification of single photon emission from hBN using post-processing treatments," *Nanophotonics*, vol. 8, no. 11, pp. 2049–2055, 2019.
[169] A. L. Exarhos, D. A. Hopper, R. R. Grote, et al., "Optical signatures of quantum emitters in suspended hexagonal boron nitride," *ACS Nano*, vol. 11, pp. 3328–3336, 2017.
[170] N.R. Jungwirth, and G.D. Fuchs, "Optical absorption and emission mechanisms of single defects in hexagonal boron nitride," *Phys. Rev. Lett.*, vol. 119, 2017, 057401.
[171] X. Li, G. D. Shepard, A. Cupo, et al., "Nonmagnetic quantum emitters in boron nitride with ultranarrow and sideband-free emission spectra," *ACS Nano*, vol. 11, pp. 6652–6660, 2017.
[172] F. Hayee, L. Yu, J. L. Zhang, et al., "Revealing multiple classes of stable quantum emitters in hexagonal boron nitride with correlated optical and electron microscopy," *Nat. Mater.*, vol. 19, pp. 534–539, 2020.
[173] J. R. Reimers, A. Sajid, R. Kobayashi, and M. J. Ford, "Understanding and calibrating density-functional-theory calculations describing the energy and spectroscopy of defect sites inhexagonal boron nitride," *J. Chem. Theory Comp.*, vol. 14, pp. 1602–1613, 2018.
[174] E. F. Gross, and D. S. Nedzvetskii, "Regularly converging line luminescence in GaP crystals," , 154, E. F. Gross, and D. S. Nedzvetskii, Eds., Soviet Phys. Doklady, 1964, pp. 64–67. English translation :1964 ;9 :38-42 . They interpreted their fantastic results in terms of Donor-Acceptor Pairs, as not so much was known regarding short-range impurity potentials at that time. Dokl. Akad. Nauk SSSR1.
[175] F. Schubert, Ed., *Light Emitting Diodes*, New York, Melbourne, Madrid, Cape Town, Singapore, São Paulo, Cambride University Press-Cambridge, 2006, -13 978-0-521-86538-8.
[176] D. G. Thomas, J. J. Hopfield, and C. J. Frosch, "Isoelectronic traps due to nitrogen in Gallium phosphide," *Phys. Rev. Lett.*, vol. 15, pp. 857–860, 1965.
[177] P. R. C. Kent, and Alex Zunger, "Evolution of III-V nitride alloy electronic structure: the localized to delocalized transition," *Phys. Rev. Lett.*, vol. 86, pp. 2613–2616, 2001. nd their other joint papers.
[178] M. Kneissl, T. Y. Seong, J. Han, and H. Amano, "The emergence and prospects of deep-ultraviolet light-emitting diode technologies," *Nat. Photonics*, vol. 13, no. 4, pp. 233–244, 2019.
[179] A. K. Geim, and I. V. Grigorieva, "Van der Waals heterostructures," *Nature*, vol. 499, pp. 419–425, 2013.